Title

- The role of satellite cell-derived TRIM28 in mechanical load- and injury-induced myogenesis

- Short Title: TRIM28 controls fusion pore formation during myogenesis

Authors

Kuan-Hung Lin[1,2,3,†], Jamie E. Hibbert[1,2,†], Jake L. Lemens[1,2], Melissa M. Torbey[1,2], Nathaniel D. Steinert[1,2], Philip M. Flejsierowicz[1,2], Kiley M. Melka[1,2], Marcos Lares[4], Vijayasaradhi Setaluri[4], and Troy A. Hornberger[1,2,*]

Affiliations

[1] Department of Comparative Biosciences, University of Wisconsin - Madison, WI, USA
[2] School of Veterinary Medicine, University of Wisconsin - Madison, WI, USA
[3] Department of Stem Cell and Regenerative Biology, Harvard University, Cambridge, MA, USA
[4] Department of Dermatology, University of Wisconsin - Madison, WI, USA
[†] These authors contributed equally

*Corresponding author: Troy A. Hornberger
2015 Linden Drive
Madison WI, 53706
Phone: (608) 890-2174
Email: troy.hornberger@wisc.edu

Abstract

Satellite cells are skeletal muscle stem cells that contribute to postnatal muscle growth, and they endow skeletal muscle with the ability to regenerate after a severe injury. Here we discovered that this myogenic potential of satellite cells requires a protein called tripartite motif-containing 28 (TRIM28). Unexpectedly, multiple lines of both *in vitro* and *in vivo* evidence revealed that the myogenic function of TRIM28 is not dependent on changes in the phosphorylation of its serine 473 residue. Moreover, the functions of TRIM28 were not mediated through the regulation of satellite cell proliferation or differentiation. Instead, our findings indicate that TRIM28 regulates the ability of satellite cells to progress through the process of fusion. Specifically, we discovered that TRIM28 controls the expression of a fusogenic protein called myomixer and concomitant fusion pore formation. Collectively, the outcomes of this study expose the framework of a novel regulatory pathway that is essential for myogenesis.

Teaser

TRIM28 regulates the induction of myomixer expression and fusion pore formation during myogenesis.

Introduction

As the largest tissue in the body, skeletal muscle comprises approximately 40% of total mass and plays an essential role in breathing, mobility, whole-body metabolism, and maintaining a high quality of life (*1, 2*). Notably, adults will lose approximately 35-40% of their muscle mass between the ages of 25 and 80 years (*3*). This gradual loss of muscle is not only associated with decreased independence, disability, and mortality but also an estimated 40 billion dollars in annual healthcare costs in the United States alone (*4, 5*). Therefore, developing therapies that can maintain or restore muscle mass is of great clinical and fiscal significance. However, to develop such therapies, a comprehensive understanding of the molecular mechanisms that regulate this system is needed.

It is well established that skeletal muscles possess a remarkable ability to adapt their mass in response to conditions such as an increase in mechanical loading, and they are also capable of regenerating after an injury (*6, 7*). At the cellular level, the mechanical load-induced increase in muscle mass is thought to be driven by an increase in the size of the pre-existing myofibers, whereas regeneration is driven by the formation of new myofibers (*8, 9*). Importantly, a class of skeletal muscle stem cells called satellite cells have been implicated in the regulation of both processes (*10, 11*). Specifically, in mature skeletal muscle, satellite cells are quiescent but they can be activated by stimuli such as an increase in mechanical loading or injury (*12, 13*). Once activated, satellite cells will express a critical myogenic transcription factor called the myoblast determination protein (MYOD), and then enter the cell cycle to expand their population (*14, 15*). Most of the proliferated satellite cells will then differentiate into myoblasts and contribute to myogenesis by undergoing heterotypic fusion (the fusion between a myoblast and myofiber) or homotypic fusion (the fusion between myoblasts) which will give rise to the accretion of new myonuclei in pre-existing myofibers or the formation of new myofibers, respectively (*16-18*).

Satellite cells, like all other cells in the body, express tripartite motif-containing 28 (TRIM28) (*19, 20*). TRIM28 functions as a global genome transcription intermediary factor and it has been reported to be involved in a variety of biological events, including embryonic and stem cell development, cell cycle regulation, tumorigenesis, repression of endogenous retroviruses, and of particular interest for this study, myogenesis (*21-24*). Specifically, a previous study in C2C12 myoblasts reported that the changes in TRIM28(S473) phosphorylation can act as a switch that regulates the ability of MYOD to drive myogenesis *in vitro* (*23*). We were intrigued by this possibility because recent phosphoproteomic analyses from our lab revealed that an increase in mechanical loading leads to a robust increase in TRIM28(S473) phosphorylation and therefore suggested that TRIM28 might serve as a critical regulator of myogenesis *in vivo* (*25, 26*). Thus, the overarching goal of this study was to address this possibility

Results

Maximum intensity contractions induce TRIM28(S473) phosphorylation in satellite cells

To identify phosphorylation events that regulate skeletal muscle growth, our lab performed two different phosphoproteomic-based studies on mouse tibialis anterior (TA) muscles that had been subjected to increased mechanical loading via a bout of maximal-intensity contractions (MICs). In both studies, changes in TRIM28(S473) phosphorylation were identified as one of the most robustly regulated events (*25, 26*), and as shown in Fig. 1 A-C, we extended those findings by showing that the induction of TRIM28(S473)

phosphorylation could be detected in myonuclei as well as within the nuclei of a subset of the interstitial cells. Intrigued by this finding, and the report that TRIM28(S473) phosphorylation regulates myogenesis *in vitro* (*23*), we performed additional immunohistochemical analyses to determine whether MICs induce TRIM28(S473) phosphorylation within satellite cells. As shown in Fig. 1 D-E, we found that MICs lead to a robust increase in the percentage of satellite cells that were positive for TRIM28(S473) phosphorylation and therefore suggested that changes in TRIM28(S473) phosphorylation might play a key role in regulating the myogenic effects of mechanical loading.

Characterization of tamoxifen-inducible and satellite cell-specific TRIM28 knockout mice.

To define the role of TRIM28 in myogenesis, we generated tamoxifen-inducible and satellite cell-specific *Trim28* knockout mice by crossing *Trim28*$^{flox/flox}$ mice with Pax7-iCre$^{+/-}$ mice (*24, 27*). Offspring with a genotype of Pax7-iCre$^{+/-}$: *Trim28*$^{flox/flox}$ were used for the knockout group (KO), and those with a genotype of Pax7-iCre$^{-/-}$: *Trim28*$^{flox/flox}$ were used for the control group (WT). To establish the specificity and efficiency of the knockout, we collected plantaris muscles from the WT and KO mice 14 days after they had been treated with tamoxifen. As shown in Fig. 1F-G, immunohistochemical analysis revealed that >98% of the satellite cells in the plantaris muscles from the KO mice were TRIM28 negative, whereas the expression of TRIM28 remained readily detectable in Pax7 negative cells. Importantly, we also determined that the number of satellite cells per myofiber was not altered in the KO condition which indicates that the loss of TRIM28 in satellite cells did not impact satellite cell viability (Fig. 1H).

The loss of TRIM28 does not alter the mechanical load-induced proliferation or differentiation of satellite cells.

Having confirmed the specificity and efficiency of the KO mice, our next goal was to determine whether TRIM28 plays a role in mechanical load-induced myogenesis. To accomplish this, we subjected tamoxifen-treated WT and KO mice to a unilateral synergist ablation (SA) surgery in which the soleus and distal 2/3^{rds} of the gastrocnemius muscles were surgically removed in one hindlimb, while a sham (control) surgery was performed on the contralateral hindlimb. Plantaris muscles were collected at 4 days post SA and subjected to immunohistochemical analysis for Ki67 which serves as a marker of proliferating cells (*28, 29*). As shown in Fig. 2A-B, we determined that SA led to a substantial increase in the number of Ki67 positive satellite cells, and this effect was not impacted by the loss of TRIM28. We also subjected the same samples to immunohistochemical analysis of myogenin (MYOG) which serves as a marker of satellite cells that have differentiated into myoblasts. As expected, the outcomes revealed that SA led to a significant increase in the number of MYOG-positive cells per myofiber, but again, this effect was not impacted by the loss of TRIM28 (Fig. 2C-D). Collectively, these results indicate that TRIM28 is not required for the mechanical load-induced proliferation or differentiation of satellite cells.

The loss of TRIM28 in satellite cells attenuates mechanical load-induced myonuclear accretion but it does not alter the increase in muscle mass or myofiber size.

Current models assert that when mechanical loads induce the activation of satellite cells, the satellite cells will proliferate, differentiate, and then engage in heterotypic fusion with the pre-existing myofibers (*13, 30-32*). As reported in Fig. 2, the loss of TRIM28 did not impact the mechanical load-induced activation of satellite cell proliferation or differentiation, however, these experiments did not address whether TRIM28 was required

for the induction of heterotypic fusion / myonuclear accretion. Therefore, to address this, WT and KO mice were subjected to SA and treated with daily injections of 5-bromo-2'-deoxyuridine (BrdU) for 14 days. BrdU labels DNA that has undergone replication, and since myonuclei have been shown to replicate DNA at an extremely low rate (*33*), the vast majority of BrdU-labeled myonuclei should be representative of satellite cells that have undergone proliferation, differentiation, and subsequent heterotypic fusion (*31, 34*). As illustrated in Fig. 3A, the outcomes of this experiment revealed that SA led to a substantial increase in the number of BrdU-positive myonuclei, and the magnitude of this effect was significantly lower in the muscles of KO mice. We also determined that SA led to an increase in the number of myonuclei per myofiber, and again, the magnitude of this effect was significantly lower in the muscles of the KO mice (Fig. 3B). Since the loss of TRIM28 did not appear to alter the mechanical load-induced activation of satellite cell proliferation or differentiation (Fig. 2A-B), the most likely explanation for these results was that the loss of TRIM28 inhibited the process of heterotypic fusion. However, alternative explanations such as TRIM28 being required for the post-differentiation survival of the satellite cells cannot be ruled out.

In conjunction with their role in myonuclear accretion, many studies have asserted that the satellite cell-dependent accretion of myonuclei is required for the mechanical load-induced growth of skeletal muscle (*35-37*). As such, we reasoned that the reduced myonuclear accretion in the KO muscles would lead to impaired growth. However, as shown in Fig. 2D-F, we determined that the loss of TRIM28 did not alter the mechanical load-induced increase in mass or cross-sectional area (CSA) of the Type II myofibers (See Fig. S1 for Type IIa, IIx, and IIb specific data). However, many of the myofibers in the KO muscles that had been subjected to SA had an abnormal appearance of dystrophin, and this effect was not observed in the sham (control) muscles or in the muscles from WT mice that had been subjected to SA (Fig. S2). The abnormal appearance of dystrophin was similar to what has been described in various skeletal muscle myopathies (*38*), and thus, although the satellite cell-specific loss of TRIM28 did not inhibit mechanical load-induced growth in terms of the changes in muscle mass and myofiber size, we cannot exclude the possibility that it may have led to functional deficits.

The loss of TRIM28 in satellite cells leads to a fusion defect during injury-induced myogenesis.

In addition to their role in the regulation of myonuclear accretion during the mechanical load-induced growth of skeletal muscle, numerous studies have also shown that satellite cells are required for the successful regeneration of skeletal muscle following an injury (*39-41*). Hence, we next sought to determine whether TRIM28 plays a role in injury-induced myogenesis/regeneration. To accomplish this, one TA muscle from each WT and KO mouse was injected with $BaCl_2$ to induce injury (*42*), whereas the contralateral TA was injected with phosphate-buffered saline (PBS) as a control condition. The number of MYOD-positive nuclei at 3 days post-injury (dpi) was then used to assess satellite cell activation and proliferation. As illustrated in Fig. S3A-B, the injury led to a dramatic increase in the number of MYOD-positive nuclei, and this effect was not altered by the satellite cell-specific loss of TRIM28. Thus, consistent with the results from the SA model, it can be concluded that TRIM28 is not required for the activation and subsequent proliferation of satellite cells.

Next, we wanted to determine whether the satellite cell-specific loss of TRIM28 would impact the regeneration of the injured muscles. Hence, TA muscles were collected at 5, 7, 10, and 21 dpi, and subjected to immunohistochemistry for embryonic myosin heavy chain

(eMHC) which serves as a marker of differentiated myoblasts and/or regenerating myofibers (Fig. 4A) (*43, 44*). In the TA muscles from WT mice, numerous small positive and centrally nucleated myoblasts/myofibers were detected at 5 and 7 dpi. By 10 dpi, the majority of the myofibers were eMHC negative and the overall CSA of the myofibers had substantially increased. Finally, by 21 dpi, nearly all of the myofibers were eMHC negative, and aside from central nucleation, they were indistinguishable from the myofibers in the control muscles (Fig. 4A - Top Row). Similar to WT mice, the injured muscles of KO mice also contained numerous small eMHC positive and centrally nucleated myoblasts/myofibers at 5 and 7 dpi (Fig. 4A - Bottom Row). However, by 10 dpi, the appearance of the WT and KO muscles became markedly different. Specifically, unlike WT muscles, the vast majority of the myoblasts/myofibers in the KO muscles remained eMHC positive and had a very small CSA. By 21 dpi, the difference between the WT and KO muscles became even more extreme, with the previously injured region in the KO muscles showing a dense infiltration of nuclei that was largely devoid of myoblasts/myofibers.

Qualitatively, the impaired regenerative ability of the KO muscles became readily apparent by 10 dpi, and since the loss of TRIM28 had previously been reported to inhibit the differentiation-induced expression of MYOG *(23)*, we reasoned that the impaired regenerative response might be due to a failure in the ability of the satellite cells to differentiate into myoblasts (i.e., become MYOG positive). However, as mentioned above, the presence of eMHC serves as a marker of differentiated myoblasts, and no apparent difference in the number of eMHC-positive myoblasts/myofibers was observed at 5 and 7 dpi in the WT versus KO muscles. Moreover, we found that the number of MYOG-positive nuclei per unit area at 10 dpi in KO muscles was actually 14-fold higher than in WT muscles (Fig. S4A-B). Accordingly, our results provided further support for the notion that TRIM28 is not required for the differentiation of satellite cells.

During regeneration, differentiated myoblasts align with each other and then fuse to form new myofibers. After the new myofibers have been formed, additional fusion events will occur until the new myofibers have grown to a mature size (*45*). As mentioned above, one of the first notable differences between the WT and KO muscles was that the size of the myoblasts/myofibers in the WT muscles increased between 7 and 10 dpi, but the increase in size did not occur in the KO muscles. Based on this observation, as well as our previous results with the SA model, we suspected that the loss of TRIM28 might led to a defect at the level of fusion. Hence, to further pursue this, we looked more closely at muscles 7 dpi and found that both WT and KO muscles were highly enriched with clusters of well-aligned eMHC-positive myoblasts/myofibers that were surrounded by a thick outer layer of laminin. Importantly, however, in the KO muscles, a much higher proportion of these clusters contained myoblasts/myofibers with a dense wall of filamentous actin between the aligned cells (Fig. S5). Previous studies have shown that, prior to fusion, dense walls of filamentous actin appear between the aligned cells, and then, as fusion progresses, the walls of filamentous actin break down (*46, 47*). Accordingly, the results in Fig. S5 suggested that the loss of TRIM28 may have inhibited the ability of the myoblasts to either engage in and/or complete the process of fusion.

To more thoroughly characterize the putative fusion defect, myoblasts/myofibers at 5, 7, and 10 dpi were categorized as being in one of the following stages: fusing, fused, mature, or pre-existing (Fig. 4B-E), and then the proportion in each stage was determined. As shown in Fig. 4F, all of the myoblasts/myofibers in WT and KO muscles at 5 dpi were categorized as “fusing” or “fused”. By 10 dpi, the myoblasts/myofibers in WT muscles had transitioned to the point at which >75% were categorized as “mature” myofibers. However, in the KO muscles, almost no “mature” myofibers were identified, instead, >96% of the

myoblasts/myofibers were still categorized as "fusing". Thus, these results provided further evidence for the notion that the loss of TRIM28 inhibits the ability of the myoblasts/myofibers to complete the process of fusion that occurs between 7-10 dpi. Of note, previous studies have reported that myoblasts will die if they do not undergo fusion (*48, 49*), and given the results in Fig. 4F, this likely explains why KO muscles at 21 dpi were largely devoid of myoblasts/myofibers.

The loss of TRIM28 in satellite cells leads to a profound functional deficit and excessive fibrosis following $BaCl_2$-induced injury.

The above results indicated that, at the cellular level, injury-induced myogenesis/regeneration is severely impaired by the satellite cell-specific loss of TRIM28. To determine whether this impairment translated into a functional deficit, the mass and force-producing capabilities of the muscles were measured. As shown in Fig. 5, the outcomes revealed that, in WT muscles, peak tetanic force production was 64% lower at 7 dpi and this loss was restored to control levels by 21 dpi. However, in KO muscles, force production was 95% lower at 7 dpi, and very little, if any, recovery was observed at 21 dpi. In line with these results, we also found that the mass and gross appearance of the WT muscles at 21 dpi were very similar to the control muscles, but the KO muscles were markedly small and pale in color.

The pale color of the KO muscles suggested that they might suffer from excessive fibrosis (*50*), and this was substantiated by Sirius Red staining which revealed that the proportion of the muscles that were occupied by collagen progressively increased following injury in the KO mice (Fig. S6A-B). This was intriguing because excessive fibrosis has been widely associated with aberrant regeneration (*51*). Moreover, previous studies have reported that the secretion of miR-206 by satellite cells can inhibit the expression of collagen by fibroblasts and that TRIM28 is required for the differentiation-induced expression of miR-206 (*23, 52*). Thus, we envisioned that the satellite cell-specific loss of TRIM28 might predispose the KO muscles to a miR-206-dependent increase in fibrosis and, in turn, inhibit the ability of the myoblasts/myofibers to progress through the process of fusion. Accordingly, we tested this by treating the mice with Nilotinib, which is a drug that has been shown to reduce fibrosis in chronically injured muscles (*53*). As reported in Fig. S6C-D, Nilotinib led to a 50% reduction in the area of the KO muscles that were occupied by collagen at 10 dpi: however, the proportion of myoblasts/myofibers that had progressed beyond the stage of "fusing" was only slightly improved (Fig. S6E-F). Thus, although our data indicates that the satellite-cell specific loss of TRIM28 leads to excessive fibrosis, this effect does not appear to be a major driver of the impaired fusion that is observed in KO muscles.

The loss of TRIM28 in primary myoblasts leads to a fusion defect.

To more clearly define the role that TRIM28 plays in fusion, we isolated primary myoblasts from WT and KO mice. After confirming that the primary myoblasts from the KO mice were negative for TRIM28 (Fig. S7A-B), they were subjected to a myotube formation assay and the differentiation index (i.e., the proportion of nuclei that were inside myosin heavy chain (MHC) positive cells) and fusion index (i.e., the proportion of nuclei that were inside MHC positive multinucleated cells) were measured. As shown in Fig. S7C-E, the outcomes revealed that the KO primary myoblasts had a slightly lower differentiation index along with a dramatically lower fusion index. These observations were consistent with our *in vivo* results and further suggested that TRIM28 plays an important role in the process of fusion. However, for reasons that are not clear, the KO primary myoblasts were difficult

to propagate and this prevented us from performing additional mechanistic studies (Fig. S7F).

To overcome the propagation defect we switched to a shRNA-mediated knockdown system. Specifically, WT primary myoblasts were infected with lentivirus encoding a scrambled shRNA (CNT) or shRNA targeting *Trim28* mRNA (KD). As shown in Fig. 6A-B, infection with KD shRNA led to a clear reduction in the protein level of TRIM28 when the cells were cultured in growth media and this effect was maintained after the cells had been induced to differentiate for 2 days. In agreement with our *in vivo* analyses, we also found that the knockdown of TRIM28 did not significantly alter the expression of MYOD or the differentiation-induced increase in MYOG (Fig. 6C-D). Moreover, our myotube formation assay revealed that the knockdown of TRIM28 did not significantly impact the differentiation index but, once again, it did lead to a severe reduction in the fusion index (Fig. 6E-G). Finally, as shown in Fig. 6H, we also determined that the cells infected with KD shRNA did not suffer from a propagation defect, and therefore, we were confident that the knockdown system would enable us to gain further insight into why TRIM28 is necessary for myoblasts to either engage in and/or complete the process of fusion.

TRIM28(S473) phosphorylation is not required for myoblast fusion *in vitro.*

Collectively, our *in vivo* and *in vitro* analyses strongly suggested that TRIM28 is not required for myoblast differentiation (Figs. 2C-D, 4A, 6E-F). Yet, TRIM28 clearly played a major role in the regulation of myogenesis, and it appeared that this was due to its ability to regulate fusion. Consistent with this point, it was previously reported that the loss of TRIM28 significantly inhibits myotube formation in C2C12 myoblasts: however, the same study also concluded that TRIM28 exerts its functions via the regulation of differentiation (*23*). For instance, using the same shRNA constructs that we employed, it was determined that the knockdown of TRIM28 in C2C12 myoblasts inhibited the differentiation-induced increase in the expression of critical regulators of differentiation such as MYOG. Moreover, it was concluded that the ability of TRIM28 to regulate differentiation was dependent on TRIM28(S473) phosphorylation. This is important because, as shown in Fig. 1, our interest in TRIM28 began with the observation that myogenic stimuli, such as increased mechanical loading, lead to a very robust increase in TRIM28(S473) phosphorylation. As such, we wanted to determine whether the role that TRIM28 plays in the regulation of myogenesis/fusion is dependent on changes in S473 phosphorylation. Thus, to address this, WT primary myoblasts were subjected to a rescue-based experiment in which shRNA-mediated knockdown of endogenous TRIM28 was coupled with "rescue" expression of an shRNA-resistant form of wild-type TRIM28 (KD + WT) or an shRNA-resistant and phosphodefective form of TRIM28 (KD + PD) in which the serine 473 residue had been mutated to a non-phosphorylatable alanine.

The rescue-based approach that we employed utilized the same lentiviral constructs that were used in a previous study with C2C12 myoblasts (*23*), and the first thing we noticed was that the transduction efficiency of the "rescue" constructs (i.e, KD + WT and KD + PD) was quite low when compared with the efficiency of the CNT and KD constructs. Nevertheless, we were able to culture enough myoblasts to conduct myotube formation assays and, as expected, expression of the shRNA-resistant form of wild-type TRIM28 (i.e., KD + WT) was able to rescue the fusion defect that was observed in the KD condition (Fig. S8). However, much to our surprise, expression of the shRNA-resistant and phosphodefective form of TRIM28 (i.e., KD + PD) also rescued the fusion defect (Fig. S8).

The results in Fig. S8 suggested that TRIM28(S473) phosphorylation is not required for the role that TRIM28 plays in the regulation of fusion and this is very different from the observations that were reported in C2C12 myoblasts (*23*). We were puzzled by this discrepancy, and since both of our studies employed the same constructs, we reasoned that the discrepancy might be due to the fact that we employed primary myoblast. Hence, to test this, we tried to repeat our studies in C2C12 myoblasts. However, just like with the primary myoblasts, we found that the transduction efficiency of the KD + WT and KD + PD constructs was very low. Indeed, despite several attempts, the low transduction efficiency prevented us from being able to culture enough C2C12 myoblasts to conduct myotube formation assays. As such, we were not able to establish whether the discrepancy in our observations could be attributed to differences in C2C12 myoblasts versus primary myoblasts.

A novel *in vivo* "rescue" approach reveals that TRIM28(S473) phosphorylation in satellite cells is not required for injury-induced myogenesis/regeneration.

Given the difficulties that were encountered with the *in vitro* rescue-based experiments, we were only moderately convinced that TRIM28(S473) phosphorylation does not play a role in the regulation of fusion. Moreover, since the shRNA-mediated knockdown studies relied on the use of *in vitro* conditions, they could not provide definitive insights into the role that TRIM28(S473) phosphorylation plays *in vivo.* Hence, to overcome these limitations, we developed a innovative genome editing strategy that enabled us to perform rescue-based experiments *in vivo*. Specifically, we created mice that allowed for tamoxifen-inducible and satellite cell-specific knockout of endogenous TRIM28 along with simultaneous satellite cell-specific and tamoxifen-inducible "rescue" expression of human TRIM28 (KO + hTRIM28) or a S473A phosphodefective mutant of hTRIM28 (KO + hTRIM28(S473A)) (Fig. S9 and 7A-B).

To create the KO + hTRIM28 mice, a construct encoding HA-tagged hTRIM28 (HA-hTRIM28) downstream of a LoxP-Stop-LoxP (LSL) cassette was knocked into the H11 locus of TARGATT^{TM} C57BL6 mice (*54*) (Fig. S9A-B). These mice were then crossed with KO mice to create KO + hTRIM28 progeny with a genotype of *Pax7*-iCre$^{+/-}$: *Trim28*$^{flox/flox}$: LSL-HA-hTRIM28$^{+/+}$. To create the KO + hTRIM28(S473A) mice, CRISPR-Cas9-mediated homologous-directed repair was used to make a single point mutation in hTRIM28 of the TARGATT LSL-HA-hTRIM28 mice. The single point mutation converted the serine 473 residue of hTRIM28 to a non-phosphorylatable alanine, and these mice were crossed with KO mice to create KO + hTRIM28(S473A) progeny with a genotype of *Pax7*-iCre$^{+/-}$: *Trim28*$^{flox/flox}$: LSL-HA-hTRIM28(S473A)$^{+/+}$ (Fig. S9C-D).

To assess whether the "rescue" expression of HA-hTRIM28 in the KO + hTRIM28 and KO + hTRIM28(S473A) mice was working appropriately, TA muscles were collected 14 days after mice had been treated with tamoxifen and assessed for the presence of HA positive satellite cells. As expected, HA-positive satellite cells were widely abundant in the muscles from KO + hTRIM28 and KO + hTRIM28(S473A) mice, but not in the muscles from WT and KO mice (Fig. 7C). With these results in hand, we next set out to establish whether the expression of hTRIM28 and/or hTRIM28(S473A) could rescue the fusion defect that occurs in muscles of KO mice at 10 days after $BaCl_2$-induced injury. Consistent with the results presented in Fig. 4, we found the vast majority of the myoblasts/myofibers in WT muscles were categorized as "mature" myofibers at 10 dpi, whereas almost no "mature" myofibers were identified in the muscles of the KO mice (Fig. 7D-E). Importantly, the expression of hTRIM28 in the KO mice completely rescued this defect, and the same point was true for the expression of hTRIM28(S473A).

The results in Fig. 7 reinforced the validity of the observations that were made with our *in vitro* rescue-based studies, and further demonstrated that changes in TRIM28(S473) phosphorylation are not required for the role that TRIM28 plays in the regulation of fusion. To extend these observations we also assessed whether any of the roles that TRIM28 plays in myogenesis/regeneration are dependent on S473 phosphorylation (e.g., restoration of myofiber CSA, force production, etc.). Specifically, TA muscles from WT, KO, KO + hTRIM28, and KO + hTRIM28(S473A) mice were injected with $BaCl_2$ or PBS and collected at 21 dpi. Consistent with the results in Fig. 5, we found that injured KO muscles were small and pale in color at 21 dpi, but such effects were not observed in the injured muscles of the KO + hTRIM28 or KO + hTRIM28(S473A) mice (Fig. 8A-B, see Fig. 5E for representative images of WT and KO muscles). Cross-sections of the TA muscles also revealed that, aside from the presence of HA-positive myonuclei, the regenerated myofibers in KO + hTRIM28 and KO + hTRIM28(S473A) muscles were indistinguishable from those of WT muscles (Fig. 8C and S10). Moreover, the force-producing ability of the muscles from KO mice was severely impaired at 21 dpi, but again, this effect was not observed in the muscles from KO + hTRIM28 or KO + hTRIM28(S473A) mice (Fig. 8D). Thus, our novel *in vivo* "rescue" approach not only enabled us to establish that TRIM28(S473) phosphorylation in satellite cells is not required for any of the events that are necessary for successful myogenesis/regeneration of skeletal muscle, but it also provided further support for the validity of our *in vitro* observations.

The loss of TRIM28 inhibits the process of fusion pore formation but not hemifusion.

Having established that the primary conclusions from the *in vitro* assays were conserved *in vivo*, we next sought to gain additional insight into the mechanism via which TRIM28 regulates fusion. To accomplish this, we turned to one of the more widely accepted models in the field which argues that fusion occurs in two major stages. Specifically, the first stage is referred to as hemifusion and involves the mixing of the outer membranes of the fusing cells (*45, 55, 56*), whereas the second stage involves the formation of a fusion pore that allows for the mixing of the intracellular contents of the fusing cells (*55, 57*). Thus, to determine whether the loss of TRIM28 affected hemifusion and/or fusion pore formation, CNT and KD myoblasts were differentiated for 24 hours, detached, and then briefly labeled with either an intracellular content probe or a lipid membrane probe (Fig. 9A). The separately labeled cells were then mixed, plated, and allowed to differentiate. After 30 hours, the cells were analyzed and mononucleated cells that were positive for both probes were classified as having only undergone hemifusion, whereas all multinucleated cells were classified as having undergone fusion pore formation. As illustrated in Fig. 9A-D, the results of our analyses revealed that the loss of TRIM28 did not significantly alter the proportion of the nuclei that resided within cells that had only undergone hemifusion, but it did lead to a highly significant reduction in the proportion of nuclei that resided within cells that had undergone fusion pore formation.

Previous studies have identified two muscle-specific fusogenic proteins that play a critical role in fusion and these proteins are generally referred to as myomaker (MYMK, also known as TMEM8C) and myomixer (MYMX, also known as myomerger and MINION) (*58-61*). Recent *in vitro* studies have shown that MYMK is required for hemifusion and that fusion pore formation will not occur if either of the two fusing cells lacks it (*45, 55, 62*). On the other hand, MYMX is thought to physically drive the process of fusion pore formation, and unlike with MYMK, fusion pore formation is only partially inhibited if either of the two fusing cells lacks MYMX (*60, 62*). Since the results in Fig. 9A-D indicated that the loss of TRIM28 impairs fusion pore formation but not hemifusion,

we suspected that the loss of TRIM28 would regulate fusion pore formation in a manner that is analogous with the functions of MYMX (i.e., fusion pore formation would only be partially inhibited if one of the two fusing cells lacked it). Hence, to test this, CNT and KD primary myoblasts were differentiated for 24 hours, detached, and then briefly labeled with a red- or green-fluorescent intracellular content probe. The separately labeled cells were then mixed into one of the following types of pairs: CNT-red with CNT-green, CNT-red with KD-green, or KD-red with KD-green (Fig. 9E-F). Fusion pore formation as a result of heterologous fusion was then quantified by identifying multinucleated cells that were positive for both of the intracellular content probes. As shown in Fig. 9E-G, the magnitude of fusion pore formation was maximal when both cells expressed a normal level of TRIM28, it was partially inhibited when only one cell expressed a normal level of TRIM28, and it was largely abolished when both cells suffered from the loss of TRIM28. These outcomes are extremely similar to what has previously been reported with the loss of MYMX in human primary myoblasts and therefore suggested that TRIM28 regulates fusion via a MYMX-dependent mechanism (*62*).

The loss of TRIM28 inhibits the induction of MYMX expression during differentiation and injury-induced myogenesis.

Previous studies have shown that the induction of differentiation leads to an increase in the expression of MYMX and MYMK, and the results in Fig. 9 revealed that the loss of TRIM28 inhibits the process of fusion pore formation but not hemifusion (*58-61*). Accordingly, we suspected that the loss of TRIM28 would inhibit the differentiation-induced increase in MYMX expression, but not MYMK. To test this, lysates from the CNT and KD primary myoblasts described in Fig. 6A-B were subjected to western blot analysis for MYMX and MYMK. As shown in Fig. 10A-C, the results indicated that the knockdown-mediated loss of TRIM28 did not affect the differentiation-induced increase in MYMK. However, the differentiation-induced increase in MYMX was substantially reduced. We also discovered the differentiation-induced increase in MYMX was very highly correlated with the level of TRIM28 in the cells (Fig. 10C-D). Moreover, we examined the level of MYMX in the TA muscles of WT and KO mice that had been injured with $BaCl_2$ and as shown in Fig. 10E-F, the outcomes revealed that injury led to a robust increase in MYMX and that this effect was largely abolished by the loss of TRIM28. Thus, the results of our analyses, along with the *a priori* knowledge about myomixer, have led us to the conclusion that TRIM28 regulates myogenesis by controlling the induction of myomixer expression and concomitant fusion pore formation.

Discussion

The overarching goal of this study was to determine whether TRIM28 is a critical regulator of myogenesis. This was viewed as an important goal because myogenesis plays a vital role in the regulation of skeletal muscle mass, and the maintenance of muscle mass is essential for mobility, breathing, whole-body metabolism, and overall quality of life (*1, 2*). Moreover, skeletal muscles are one of the few mammalian tissues that are capable of regenerating, and the process of regeneration recapitulates many aspects of embryonic myogenesis (*63, 64*). Indeed, impairments in myogenesis/regeneration are associated with the progression of diseases such as muscular dystrophy and contribute to the age-related decline in the ability of skeletal muscle to recover from injury (*65, 66*). Thus, advancements in our understanding of the mechanisms that regulate myogenesis might not only lead to the development of therapies for treating these conditions, but they could also provide pivotal insights for the broader field of regenerative medicine.

By using a variety of *in vitro* and *in vivo* models we established that, in satellite cells, TRIM28 plays a critical role in the regulation of myogenesis. Surprisingly, however, we also determined that the function of TRIM28 is not mediated through changes in TRIM28(S473) phosphorylation. To reach this conclusion, we first performed *in vitro* studies with lentiviral mediated expression of shRNA targeting *Trim28* mRNA along with "rescue" expression of wild-type or serine 473 phosphodefective TRIM28. The outcomes of this approach revealed that the shRNA-mediated loss of TRIM28 substantially inhibited the ability of primary myoblasts to form myotubes, and that this defect could be rescued by the expression of either wild-type or phosphodefective TRIM28 (Fig. S8). Combined, these results indicated that changes in TRIM28(S473) phosphorylation are not required for the role that TRIM28 plays in myotube formation. Numerically, the data were very compelling: however, the results starkly contrasted with observations that were previously made in C2C12 myoblasts (*23*). To address this discrepancy, we attempted to repeat the "rescue" studies in C2C12 myoblasts, but these experiments were confounded by a very low transduction efficiency. Importantly, with the lentiviral transduction system that was employed, the transduction efficiency could significantly alter the outcomes because it will affect the level of both the virus-encoded shRNA and protein. Thus, in addition to differencs in the model systems (C2C12 myoblast vs. primary myoblast), differences in the transduction efficiency could have also led to the discrepant results. Unfortunately, the cause of the low transduction efficiency was not established but previous studies have shown that TRIM28 can repress the transcription of endogenous retroviruses (*67, 68*). Since lentiviruses are a subclass of retroviruses, we suspect that the lentiviral-mediated expression of TRIM28 suppressed its own transcription and, in turn, led to low transduction efficiency (*69*). Regardless of the exact cause, it became clear that a non-retroviral strategy would be needed to more clearly establish whether changes in TRIM28(S473) phosphorylation contribute to the role that TRIM28 plays in myogenesis.

When considering potential strategies, we recognized that an ideal "rescue" approach would be one that would enable us to study the functional significance of TRIM28(S473) phosphorylation specifically within the satellite cells of adult mice. Unfortunately, however, no method for such an approach had ever been described. For instance, the *in vivo* functional significance of a phosphorylation site is typically studied by creating mice with a knockin of a phosphodefective allele, or by using CRISPR-Cas9 to generate a phosphodefective allele (*70, 71*). Importantly, both approaches are limited by the fact that the expression of the phosphodefective mutant is not cell-type specific and the expression is constitutive which, in our study, might lead to defects in critical processes such as embryonic myogenesis. As such, we developed a innovative rescue-based approach that allowed for the simultaneous satellite cell-specific and tamoxifen-inducible knockout of endogenous TRIM28 and "rescue" knockin of either wild-type or phosphodefective TRIM28 (Figs. 7 and S9). The development of this approach was important for two reasons. First, it enabled us to establish that changes in TRIM28(S473) phosphorylation do not contribute to the role that TRIM28 plays in myogenesis. Second, it provided proof-of-concept for a cell-type specific and inducible strategy that, in theory, could be used to study the functional significance of a multitude of different forms of biological regulation including genetic mutations (e.g., base substitutions, deletions, or insertions), post-transcriptional modifications (e.g., miRNA-resistant mutations), and post-translational modifications (e.g., acetylation, SUMOylation, ubiquitination, etc.). As such, we expect that our rescue-based approach will be beneficial for a wide range of fields.

Having determined that changes in TRIM28(S473) phosphorylation do not contribute to the role that TRIM28 plays in myogenesis, we wanted to gain additional insight into the mechanism(s) via which TRIM28 exerted its regulatory effect. Importantly, the results from our *in vitro* and *in vivo* models of myogenesis consistently indicated that the loss of TRIM28 does not inhibit the proliferation or differentiation of satellite cells. Instead, several lines of evidence indicated that the loss of TRIM28 leads to a defect in satellite cell fusion. For instance, we determined that TRIM28 was not required for the mechanical load-induced activation of satellite cell proliferation or differentiation, but the loss of TRIM28 did lead to a substantial decrease in myonuclear accretion which suggested that there might be an impairment at the level of satellite cell fusion (Fig. 2-3). Likewise, we found that TRIM28 was not required for the injury-induced activation of satellite cell proliferation or differentiation, but again, multiple lines of evidence suggested that the loss of TRIM28 led to a defect in fusion (Figs. 4, 7, S3-6). Similar conclusions were also reached when we studied primary myoblasts with our *in vitro* myotube formation assay (Figs. 6, S7, S8). Given the consistent outcomes from these different model systems, we sought to gain further insight into why the loss of TRIM28 inhibits fusion, and we ultimately discovered that the loss of TRIM28 inhibits the induction of MYMX expression and fusion pore formation (Figs. 9-10). Intriguingly, although the loss of TRIM28 markedly inhibited the increase in MYMX that occurred during myotube formation, it did not inhibit the increase in MYMK. This was intriguing because it has been argued that, due to their inherent membrane-remodeling activities, stringent control of MYMK and MYMX expression is needed (*72*). Thus, it bears mentioning that, during myotube formation, the expression of MYMX and MYMK are both regulated by MYOD, and that the knockout of MYOG leads to a decrease in MYMK expression but does not affect the expression of MYMX (*62*). Furthermore, previous studies have shown that MYOD and TRIM28 physically interact and that TRIM28 can regulate the function of MYOD (*23*). As such, the potential exists for a mechanism that endows satellite cells with the ability to differentially regulate the expression of MYMK and MYMX. Specifically, in this setting, MYMK expression would be regulated by MYOD/MYOG, whereas the expression of MYMX would be regulated by MYOD/TRIM28. If correct, such a mechanism would enable satellite cells to stringently control the timing of MYMK and MYMX expressions and the related processes of hemifusion and concomitant fusion pore formation.

Limitations of the study

The results of this study provide multiple lines of evidence to support the conclusion that TRIM28 regulates myogenesis by controlling fusion pore formation. However, the exact mechanism through which TRIM28 regulates this process remains to be determined. For instance, the outcomes suggest that the regulation of fusion pore formation is due, at least in part, to the ability of TRIM28 to regulate MYMX expression. However, a role for additional fusogenic factors cannot be excluded. Moreover, the mechanism(s) via which TRIM28 regulates MYMX remains to be resolved. For instance, TRIM28 is well known for its ability to control gene expression, and as suggested above, TRIM28 might regulate the expression of MYMX at the transcriptional level (*73*). However, TRIM28 could also regulate MYMX through post-translational modifications. For instance, TRIM28 possesses SUMO E3 ligase activity and this property of TRIM28 has been implicated in the regulation of the protein levels of α-Syn and tau (*74*). TRIM28 also possesses ubiquitin E3 ligase activity which has been implicated in the regulation of the protein levels of critical factors such as p53 (*73, 75*). Importantly, the SUMO and ubiquitin E3 ligase activities of TRIM28 not only have the potential to regulate the protein levels of MYMX, but such modification could also regulate the spatial localization of MYMX and other fusogenic proteins (*76, 77*).

Hence, there is much to learn about how TRIM28 regulates fusion pore formation, and this will be an important topic for future investigations.

Materials and Methods

Animals

Male and female C57BL6 mice were obtained from the University of Wisconsin-Madison Mouse Breeding Core. Tamoxifen-inducible and satellite cell-specific *Trim28* knockout C57BL6 mice were generated by crossing *Trim28*$^{flox/flox}$ (Jackson Laboratory, Stock# 018552) with *Pax7*-iCre$^{+/-}$ (Jackson Laboratory, Stock# 017763) mice. Genotyping protocols for tail DNA of these mice can be found on the Jackson Laboratory website. The TARGATT system was used to create a rescue mouse that allowed for simultaneous satellite cell-specific and tamoxifen-inducible knockout of endogenous TRIM28 and knockin "rescue" expression of HA-tagged human TRIM28 (HA-hTRIM28). Specifically, HA-hTRIM28 was removed from pKH3-TRIM28 plasmid DNA (Addgene, #45569) via digestion with NheI and MluI in CutSmart buffer (New England Biolabs). The HA-hTRIM28 construct was then ligated into the multiple cloning site (MCS) of TARGATT^{TM}6.1 (CAG – L4SL – MCS – PolyA) vector which contains a LoxP-StopP-LoxP (LSL) cassette and an attB integration sequence (Applied StemCell, #AST-3050). Embryos from TARGATT^{TM} H11 mice (Applied StemCell) which contained an attP integration site in the H11 locus were injected with ΦC31 integrase plus TARGATT^{TM}6.1-LSL-HA-hTRIM28 (*54*). The offspring with successful integration were crossed with the *Pax7*-iCre$^{+/-}$: *Trim28*$^{flox/flox}$ mice to generate (KO + hTRIM28) mice with the genotype *Pax7*-iCre$^{+/-}$: *Trim28*$^{flox/flox}$: LSL-HA-hTRIM28$^{+/+}$. CRISPR-Cas9-mediated homologous-directed repair was used to make a single point mutation in the hTRIM28 that switched the serine 473 residue to a non-phosphorylatable alanine. Specifically, a sgRNA (GGTGTGAAACG GTCCCGCTC) was designed to introduce a double-stranded break at the region corresponding to human Trim28 exon 12. A single-stranded oligodeoxynucleotide (ssODN) homology-directed repair (HDR) donor template containing a T1416 to G1416 mutation with 75 5' nucleotides and 76 3' nucleotide homology arms was used to introduce the mutation through HDR: TGAGGTCCAGGTCCAGGCGTTCAAGG CTCACTCGTGGCACCTTGCGCATAAGGCCGCTCACCTCGCCCTCACCTGcGCGG GACCGTTTCACACCTGACACATGGGGCTCTGCACTTGAGTAGGGATCATCTCC TGACCCAAAGCCATAGCCT. The ssODN HDR template and Cas9/sgRNA RNP were co-electroporated into the embryos of the TARGATT LSL-HA-hTRIM28 knockin mice. Successfully edited offspring were crossed with the *Pax7*-iCre$^{+/-}$: *Trim28*$^{flox/flox}$ mice to generate (KO + hTRIM28(S473A)) mice with the genotype of *Pax7*-iCre$^{+/-}$: *Trim28*$^{flox/flox}$: LSL-HA-hTRIM28(S473A)$^{+/+}$. PCR with primers *p1* (5' TCTACTGGAGGAGGACAA ACTGGTCAC), *p2* (5' GACGATGT AGGTCACGGTCTCGAAG) and *p3* (5' TGACACA TCCTGCCCTTACCTTACTACC), were used to confirm the knockin of hTRIM28 from tail DNA as illustrated in Fig. S8A-B. PCR with primers *p4* (5' ATTTCAGTGG GACCTCAATGCC) and *p5* (5' GTGA CAGTCCAGGTGGAAACAAA) and Bpu10I digestion (Thermo Fisher Scientific #FD1184) was used to confirm the genomic differences between the KO + hTRIM28 and the KO + hTRIM28(S473A) mice as shown in Fig. S8C-D.

All mice were given food and water *ad libitum* and kept in a room maintained at 25°C with a 12-hour light: dark cycle. Genotypes were confirmed with PCR of tail snips when the mice were 3 weeks of age and, where indicated, 6-week-old mice were given daily

intraperitoneal injections of 100 mg/kg of tamoxifen for five consecutive days as previously described (*78*). All experiments, except Fig. 1A-E (all male) were designed in a sex-balanced manner, and interventions were performed when the mice were 8 to 10 weeks of age. For all surgical interventions mice were anesthetized with 1-5% isoflurane mixed in oxygen and given an intraperitoneal injection of 0.05 µg/g of buprenorphine to relieve any procedure-induced pain. Euthanasia was performed with cervical dislocation while the mice were under isoflurane anesthesia. All animal experiments were approved by the Institutional Animal Care and Use Committee of the University of Wisconsin-Madison (#V005375).

Maximal-intensity contractions

Maximal-intensity contractions were performed in anesthetized male C57BL6 mice as previously described (*25*). In brief, the sciatic nerve of the right thigh was exposed by a small incision along the lateral edge. An electrode was then placed on the sciatic nerve and contractions were elicited by stimulating the nerve with an SD9E Grass stimulator (Grass Instruments) at 100Hz with 0.5 ms pulses at 4-7 V for a total of 10 sets of 6 contractions. Each contraction lasted for 3 seconds and was followed by a 10-second rest period. A 1 minute rest period was provided between each set. At 1 hour after the last contraction, both the right and left TA muscles were collected and immediately processed for immunohistochemistry as detailed below.

Synergist ablation

As previously described (*79*), mice were anesthetized and subjected to unilateral synergist ablation by removing the soleus and distal 2/3^{rds} of the gastrocnemius muscle. A sham surgery was performed on the contralateral hindlimb. The plantaris muscles were collected at 4 or 14 days post-surgery for immunohistochemical analysis as detailed below. As indicated in the legend for the experiments in Fig. 3, some of the mice were also given daily intraperitoneal injections of 50 µg/g BrdU (Sigma-Aldrich) that was dissolved in PBS at a concentration of 5 mg/mL.

$BaCl_2$-induced muscle injury

The right TA muscle of anesthetized mice was injected at the proximal and distal ends with 25 µL of 1.2% $BaCl_2$ (50 µL in total), while the left TA muscle was injected in the same manner with PBS as a control condition. The TA muscles were collected at the indicated time points for immunohistochemistry or western blot analysis as detailed below. For the experiments in Fig. S6C-F, the mice also received daily intraperitoneal injections of 20 mg/kg Nilotinib (Selleck Chemical) dissolved in DMSO (Thermo Fisher Scientific) at a concentration of 5 mg/mL, or 4 mL/kg DMSO as a control condition, on days 3-5 following muscle injury.

***In Situ* Muscle Contraction**

Mice were anesthetized and the TA muscle was subjected to *in situ* measurement of force production as previously described (*25*). In brief, single-pulse stimulations (60 V for 0.5 msec) were used to determine the optimal length of the muscle and then the muscles were subjected to 300 msec tetanic contractions at 100, 150, and 200 Hz with 2 minutes between each stimulation. The highest force produced during these contractions was recorded as the peak tetanic force.

721
722

Lentivirus production

723 Lentiviral plasmids encoding scrambled shRNA (CNT), shRNA targeting *Trim28* mRNA
724 (KD), shRNA targeting *Trim28* mRNA along with expression of a shRNA resistant form of
725 TRIM28 (KD + WT), or shRNA targeting *Trim28* mRNA along with expression of an
726 shRNA resistant form of phosphodefective TRIM28 (KD + PD) in which the serine 473
727 residue had been mutated to a non-phosphorylatable alanine. These lentiviral plasmids have
728 been previously described (*23*) and were kindly provided by Dr. Didier Trono (École
729 Polytechnique Fédérale de Lausanne). The lentiviral plasmids were propagated in DH5α E.
730 coli or Stbl3 E. coli with LB broth containing 60 μg/ml Ampicillin, and purified with an
731 Endofree plasmid kit.
732

733 HEK293 cells were grown to 90% confluence in 10 cm plates (Corning) with DMEM
734 (Hyclone) containing 10% fetal bovine serum (FBS) (Invitrogen). The cells were co-
735 transfected with 2 μg lentivirus packaging plasmids (pMD2.G (Addgene #12259) and 10 μg
736 psPAX2 (Addgene #12260)) along with 10 μg lentiviral plasmid with lipofectamine 3000
737 (Thermo Fisher Scientific). After 15 hours, the medium containing viral plasmids was
738 replaced with DMEM + 10% FBS and 1% penicillin/streptomycin (Hyclone), and the cells
739 were cultured for another 72 hours. After 72 hours, the viral supernatant was harvested, and
740 the virus titer was measured based on the titer of the viral protein p24 with QuickTiter™
741 Lentivirus Titer Kit (Cell Biolabs) following the manufacturer's instructions.
742

743

Primary myoblasts

744

745 To create multiple primary myoblast lines as biological replicates, we isolated primary
746 myoblasts from different mice with the following conditions. Primary myoblast lines used
747 in Fig. S7 were isolated from four pairs of WT and KO mice (sex balanced) at 14 days post
748 tamoxifen injection. Primary myoblast lines used for the TRIM28 knockdown experiments
749 in Figs. 6-8 were isolated from four 6-week-old C57BL/6J mice (sex balanced) and
750 maintained following the protocol published by Hindi *et al.* (*80*). Specifically, hindlimb
751 muscles were harvested and minced in sterile PBS containing 1% penicillin/streptomycin.
752 The minced muscles were centrifuged at 15,000 x g for 1 minute and transferred to 10 ml
753 of digestion buffer (DMEM containing 2.5% HEPES, 1% penicillin/streptomycin, and 400
754 U/ml collagenase II (Worthington Biochemical)) and placed on an orbital shaker at 100 rpm
755 for 1 hour at 37°C. Digested tissues were centrifuged at 1,500 x g for 5 minutes, and the
756 resulting pellets were resuspended in neutralizing medium (DMEM containing 10% FBS
757 and 1% penicillin/streptomycin). Resuspended cell mixtures were filtered through a 70 μm
758 strainer (Thermo Fisher Scientific) and then a 30 μm strainer (Miltenyi Biotec). The filtered
759 cell mixtures were spun at 1,500 x g for 5 minutes and resuspended in myoblast growth
760 medium (GM) (F-10 medium (Thermo Fisher Scientific) containing 20% FBS, 10 ng/ml
761 basic fibroblast growth factor (Peprotech), and 1% penicillin/streptomycin). During the
762 isolation procedure, 10 cm dishes were coated with 3 ml of 10% Matrigel (Corning) in
763 DMEM for 1 minute. Excess Matrigel was removed and then the plates were air dried for
764 20 minutes. Resuspended cell mixtures were seeded onto the Matrigel-coated dishes (the
765 entire cell mixture from 1 animal per 10 cm dish) and grown in 5% CO_2 at 37°C. At 72
766 hours post-seeding, adherent primary myoblasts and large triangular-shaped fibroblasts
767 were present. The GM was discarded to remove any unattached cells and the remaining cells
768 were gently washed with F-10 medium containing 1% penicillin/streptomycin. Adherent
769 cells were then detached by treatment with 0.25% trypsin (Mediatech) in PBS. The detached
770 cell mixture was neutralized with GM and transferred to a regular 10 cm dish for 45 minutes.
771 During this incubation, larger non-myoblast cells (e.g., fibroblasts) adhered to the bottom
772 of the dish while the majority of the primary myoblasts remained suspended in the media.

773 The unattached cell mixture was then seeded on another Matrigel pre-coated dish and
774 propagated. The cells were grown to 50-60% confluence and then the detachment plus pre-
775 plating procedure for removing non-myoblasts was repeated before further propagation. The
776 procedure for removing fibroblasts was repeated for 2-3 passages so that a myoblast purity
777 of approximately 95% was obtained. After the cell mixture was enriched by the first pre-
778 plating procedure, the cells were defined as passage 1. The primary myoblasts used for
779 knockdown and rescue-based (Figs. 6-8) were between passages 6 and 10. For the primary
780 myoblasts that were isolated from tamoxifen-injected WT and KO mice (Fig. S7), passage
781 2 cells were used for experimentation. Thus, the pre-plating procedure was only completed
782 2 times, and the myoblast purity in these experiments was approximately 80%. To account
783 for this, care was taken to ensure that fibroblasts (defined as large mononucleated triangular-
784 shaped cells with large nuclei) were not included during the quantification of differentiation
785 and fusion indices. In all cases, propagating primary myoblasts were always maintained
786 below 70% confluence to prevent differentiation.
787
788 For primary myoblast knockdown and resue-based experiments, 2.5 x 10^5 WT primary
789 myoblasts were seeded per well on 6-well plates (Corning Costar). The next day, the
790 primary myoblasts were infected at a multiplicity of infection (MOI) of 100 with WT, KD,
791 KD + WT, or KD + PD lentivirus in GM containing 8 µg/ml polybrene (EMD Millipore).
792 The virus-containing GM was replaced with regular GM at 16 hours post-infection. At 2-3
793 days post-infection (2 days for knockdown experiments (Figs. 6 and 7), and 3 days for
794 rescue-based experiments due to low transduction efficiency (Fig. 8)), the primary
795 myoblasts were selected with 2 µg/ml puromycin in GM for 72 hours. After selection, the
796 surviving primary myoblasts were subjected to the experiments described in Fig. 6-8.
797
798 **Myotube formation assay**
799
800 A total of 1.5 x 10^5 or 3 x 10^5 primary myoblasts in GM were plated per well of 24-
801 well or 6-well plates (Corning Costar) that had been pre-coated with 10% Matrigel,
802 respectively. At 1 day post-seeding for 24-well plates, or 2 days post-seeding for 6-well
803 plates, the GM was replaced with differentiation medium (DM) (DMEM containing 2%
804 horse serum (Thermo Fisher Scientific) and 1% penicillin/streptomycin). If lentivirus-
805 infected myoblasts were used, 2 µg/ml puromycin (Thermo Fisher Scientific) was added to
806 the GM and DM. After 48 hours in DM, the myoblasts/myotubes were subjected to
807 immunohistochemistry as described below.
808
809 **Intracellular content and lipid membrane probe labeling**
810
811 CNT and KD primary myoblasts that had undergone 24 hours of differentiation were
812 detached with 0.25% trypsin and resuspended in GM to neutralize trypsin. Then, the cells
813 were washed with F-10 medium 3 times to deplete FBS and finally resuspended in FBS-
814 free F-10 medium at a density of 10^6 cells/ml. Cells were then incubated with 5 µM of the
815 fluorescent lipid probe Vybrant™ DiD (Thermo Fisher Scientific) or 10 µM of the
816 intracellular content probe Green CMFDA cell tracker or Deep Red cell tracker (Thermo
817 Fisher Scientific). Cells were incubated with the probe for 20 minutes at 37°C to allow for
818 labeling. The labeled cells were then washed with GM 3 times and resuspended in DM.
819 Different combinations of the probe-labeled cells were co-plated at a 1 to 1 ratio (3.0 x 10^5
820 cells/well of a 24-well plate) as indicated in Fig. 7. The co-plated cells were maintained in
821 DM for an additional 24 – 30 hours and then subjected to immunohistochemistry as
822 described below.
823
824

Antibodies

A detailed list of the antibodies and the dilutions that were employed is provided in Table S1.

Western blot analysis

Primary myoblasts were lysed with WIK buffer [(40 mM Tris(pH 7.5), 1 mM EDTA, 5 mM EGTA, 0.5% Triton X-100, 25 mM β-glycerophosphate, 25 mM NaF, 1 mM Na_3VO_4, 10 mg/ml leupeptin, and 1 mM PMSF], and the lysates were centrifuged at 500 x g for 5 minutes at 4°C. Frozen muscle tissues were homogenized with a Polytron for 30s in ice-cold WIK buffer as previously described (*25*). A DC protein assay kit (BioRad) was used to determine the protein concentration of individual samples. Equal amounts of protein from each sample were subjected to SDS-PAGE and transferred to a PVDF membrane at 300 mA for 1 hour and 45 minutes. Immediately after the transfer step was complete, total protein loading on the PVDF membrane was stained with No-Stain™ Protein Labeling reagent (Thermo Fisher Scientific) following the manufacturer's instructions. The image acquired from this staining procedure was used to quantify the total amount of protein transferred per sample. The PVDF membrane was then further blocked with 5% milk in TBST, and incubated with primary and secondary antibodies as previously described (*78*). Of note, the myomaker antibody was pre-incubated with a PVDF membrane at 4°C overnight to eliminate non-specific binding. For visualization, membranes were incubated with ECL-prime reagent (Amersham) and imaged with a UVP Autochemi system (Analytika Jena). All western blots were quantified with ImageJ software (NIH).

Immunohistochemistry

Freshly harvested muscles were embedded in optimal cutting temperature compound (Sakura Tissue-Tek) and frozen in liquid nitrogen-chilled isopentane for 30 seconds. A cryostat at -20°C was then used to obtain 10 µm thick mid-belly cross-sections. For conditions in which P-TRIM28(S473), or Type IIa, IIx, or IIb MHC and laminin were analyzed, the sections were fixed for 10 minutes in -20°C acetone. For all other analyses, the sections were fixed at room temperature (RT) for 10 minutes in 1% paraformaldehyde (PFA) in PBS. For studies involving the analysis of myoblasts/myotubes, the cells were fixed with 4% PFA in PBS for 10 minutes at RT. Fixed cells/sections were washed with PBS and blocked with buffer A (0.5% Triton X-100 and 0.5% bovine serum albumin (BSA) in PBS) for 20 minutes at RT. For most conditions, the blocked sections were incubated with primary antibodies or Phalloidin Conjugates (Biotium) dissolved in buffer A for 1 hour at RT. However, for the analysis of Pax7 and MyoG incubations were performed overnight at 4°C. If additional primary antibodies were being used in conjunction with Pax7 or MyoG, these incubations were performed the following day for 1 hour at RT. After the incubation with primary antibodies, the sections were washed with PBS and then incubated with secondary antibodies in buffer A for one hour at RT. Sections were again washed with PBS, and when indicated, were incubated with Hoechst (BD Bioscience) for 5 minutes at RT and subjected to additional washes with PBS. The stained sections were mounted in a layer of ProLong Gold anti-fade mounting medium (Invitrogen), overlaid with a coverslip (Thermo Fisher Scientific).

In addition to the procedures described above, the protocols that involved the detection of Pax7, MYOG, or MYOD also required the use of an antigen retrieval procedure. Specifically, immediately after the PFA fixation, the sections were washed with PBS and permeabilized with 0.2% Triton X-100 in PBS for 10 minutes at RT. The sections were then

incubated with 10 mM sodium citrate pH 6.5 for 40 minutes (10 minutes at 65°C followed by 30 minutes of cooling at RT). Following the antigen retrieval procedure the sections were blocked with buffer A and subjected to the remainder of the workflow described above.

For the analysis of BrdU incorporation, fixed sections were denatured with buffer B (2N HCl plus 0.5% Triton X-100 in PBS) for 1 hour at RT and then neutralized with TBS buffer (20 mM Tris and 150 mM NaCl in water) pH 8.4 for 10 minutes at RT. The neutralized sections were then blocked with buffer A and subjected to the remainder of the workflow described above.

Sirius Red staining

Mid-belly cross-sections from TA muscles were fixed with 4% paraformaldehyde (PFA) in PBS for 10 minutes. The fixed sections were washed with distilled water and then incubated with a 0.1% Sirius Red solution (Electron Microscopy Science) for 1 hour at RT. Stained sections were washed twice with acidified water (0.5% acetic acid) for 2 minutes per wash. The sections were then dehydrated with 2 washes of 95% ethanol followed by another 2 additional washes of 100% ethanol (2 minutes per wash). Dehydrated sections were mounted in cytoseal™ XYL (Thermo Fisher Scientific).

Image analysis and quantification

For myofiber CSA measurements of the plantaris muscle, whole muscle cross-section images were captured with a Nikon 80i epifluorescence microscope. For each muscle cross-section, the CSA of at least 70 randomly selected type IIa, IIx, and IIb myofibers were measured by tracing the laminin border with Nikon NIS-Elements D software (Nikon) as previously described (*25*). The mean CSA of measured type IIa, IIx, and IIb myofibers was defined as the type II myofiber CSA. For myofiber CSA measurements in the TA muscles, images of the whole muscle cross-sections were captured with a BZ-X700 Keyence microscope and then measurements were determined using a custom CellProfiler pipeline, as previously described (*6*).

Myonuclei, interstitial nuclei, and BrdU-positive myonuclei were identified by capturing 3-5 randomly selected fields within each muscle cross-section with an inverted Leica TCS SP8 confocal laser scanning microscope. P-TRIM28(S473) positive nuclei, BrdU positive myonuclei, and total myonuclei were manually quantified by using Leica LASX software (Leica). Myonuclei were defined as nuclei that resided inside of the dystrophin boundary of individual myofibers, whereas interstitial nuclei were defined as nuclei that reside outside of the dystrophin boundary of the myofibers.

To determine the percentage of myoblasts/myofibers that were at the stage of fusing, fused, mature, or pre-existing, 3-5 randomly selected images from each muscle cross-section were captured with a Nikon 80i epifluorescence microscope and then each myoblast/myofiber in the image was categorized as described in Fig. 4B-E.

For the quantification of Sirius Red stained sections, images of whole muscle cross-sections were captured with a BZ-X700 Keyence microscope. Images were imported into ImageJ and the border of cross-sections were manually traced to clear the region outside of the cross-sections with the ''Clear Outside'' function. The trimmed images were then separated into red, green, and blue channels. In the red channel, the intensity of the Sirius Red signal within the myofibers was set as the background in the threshold intensity program of ImageJ. The area occupied by Sirius Red (Sirius Red signal above background

intensity) was then measured and used to calculate the percent of the total muscle CSA that was occupied by Sirius Red.

All other immunohistochemistry image quantifications were completed by first capturing 3-5 randomly selected fields per sample with a Nikon 80i epifluorescence microscope. The images were assessed for the elements of interest. Importantly, all quantitative analyses were performed by investigators who were blinded to the sample identification.

Statistical Analysis

Statistical significance was determined by using the Student's t-test (independent or paired), one-way ANOVA, two-way ANOVA, or two-way repeated-measures ANOVA with Student-Newman-Keuls post hoc analysis, or simple linear regression analysis, as indicated in each figure legend. An *a priori* alpha level for statistical significance was set at 0.05. Each experiment was repeated multiple times, with the number of independent samples being specified by the *n* values in the figure legend. All data sets except for Fig, 1A-E (all male) were created with an equal number of male and female samples. In data sets with $n \geq 6$ samples, individual values that resided more than 3 standard deviations away from the mean were considered to be outliers and excluded from the final analyses. All statistical analyses were performed with Prism (GraphPad Software, San Diego, CA, USA) or SigmaPlot software (Systat Software, San Jose, CA, USA).

References

1. Y. Izumiya, T. Hopkins, C. Morris, K. Sato, L. Zeng, J. Viereck, J. A. Hamilton, N. Ouchi, N. K. LeBrasseur, K. Walsh, Fast/Glycolytic muscle fiber growth reduces fat mass and improves metabolic parameters in obese mice. *Cell Metab* **7**, 159-172 (2008).
2. R. Seguin, M. E. Nelson, The benefits of strength training for older adults. *American journal of preventive medicine* **25**, 141-149 (2003).
3. I. Janssen, S. B. Heymsfield, Z. M. Wang, R. Ross, Skeletal muscle mass and distribution in 468 men and women aged 18-88 yr. *J Appl Physiol (1985)* **89**, 81-88 (2000).
4. S. Goates, K. Du, M. B. Arensberg, T. Gaillard, J. Guralnik, S. L. Pereira, Economic Impact of Hospitalizations in US Adults with Sarcopenia. *J Frailty Aging* **8**, 93-99 (2019).
5. M. Pahor, S. Kritchevsky, Research hypotheses on muscle wasting, aging, loss of function and disability. *J Nutr Health Aging* **2**, 97-100 (1998).
6. W. G. Zhu, J. E. Hibbert, K. H. Lin, N. D. Steinert, J. L. Lemens, K. W. Jorgenson, S. M. Newman, D. W. Lamming, T. A. Hornberger, Weight Pulling: A Novel Mouse Model of Human Progressive Resistance Exercise. *Cells* **10**, (2021).
7. B. M. Carlson, The regeneration of skeletal muscle. A review. *Am J Anat* **137**, 119-149 (1973).
8. K. W. Jorgenson, S. M. Phillips, T. A. Hornberger, Identifying the Structural Adaptations that Drive the Mechanical Load-Induced Growth of Skeletal Muscle: A Scoping Review. *Cells* **9**, (2020).
9. F. S. Tedesco, A. Dellavalle, J. Diaz-Manera, G. Messina, G. Cossu, Repairing skeletal muscle: regenerative potential of skeletal muscle stem cells. *J Clin Invest* **120**, 11-19 (2010).
10. C. A. Collins, I. Olsen, P. S. Zammit, L. Heslop, A. Petrie, T. A. Partridge, J. E. Morgan, Stem cell function, self-renewal, and behavioral heterogeneity of cells from the adult muscle satellite cell niche. *Cell* **122**, 289-301 (2005).

979 11. K. A. Murach, C. S. Fry, T. J. Kirby, J. R. Jackson, J. D. Lee, S. H. White, E. E. Dupont-
980 Versteegden, J. J. McCarthy, C. A. Peterson, Starring or Supporting Role? Satellite Cells
981 and Skeletal Muscle Fiber Size Regulation. *Physiology (Bethesda)* **33**, 26-38 (2018).
982 12. S. Eliazer, J. M. Muncie, J. Christensen, X. Sun, R. S. D'Urso, V. M. Weaver, A. S. Brack,
983 Wnt4 from the Niche Controls the Mechano-Properties and Quiescent State of Muscle
984 Stem Cells. *Cell stem cell* **25**, 654-665 e654 (2019).
985 13. K. A. Murach, C. S. Fry, E. E. Dupont-Versteegden, J. J. McCarthy, C. A. Peterson,
986 Fusion and beyond: Satellite cell contributions to loading-induced skeletal muscle
987 adaptation. *FASEB J* **35**, e21893 (2021).
988 14. R. N. Cooper, S. Tajbakhsh, V. Mouly, G. Cossu, M. Buckingham, G. S. Butler-Browne,
989 In vivo satellite cell activation via Myf5 and MyoD in regenerating mouse skeletal
990 muscle. *J Cell Sci* **112 (Pt 17)**, 2895-2901 (1999).
991 15. H. Yin, F. Price, M. A. Rudnicki, Satellite cells and the muscle stem cell niche.
992 *Physiological reviews* **93**, 23-67 (2013).
993 16. E. Masschelein, G. D'Hulst, J. Zvick, L. Hinte, I. Soro-Arnaiz, T. Gorski, F. von Meyenn,
994 O. Bar-Nur, K. De Bock, Exercise promotes satellite cell contribution to myofibers in a
995 load-dependent manner. *Skeletal muscle* **10**, 21 (2020).
996 17. S. M. Hindi, M. M. Tajrishi, A. Kumar, Signaling mechanisms in mammalian myoblast
997 fusion. *Science signaling* **6**, re2 (2013).
998 18. S. C. Sampath, S. C. Sampath, D. P. Millay, Myoblast fusion confusion: the resolution
999 begins. *Skeletal muscle* **8**, 3 (2018).
1000 19. M. J. Petrany, C. O. Swoboda, C. Sun, K. Chetal, X. Chen, M. T. Weirauch, N.
1001 Salomonis, D. P. Millay, Single-nucleus RNA-seq identifies transcriptional heterogeneity
1002 in multinucleated skeletal myofibers. *Nature communications* **11**, 6374 (2020).
1003 20. S. S. Kim, Y. M. Chen, E. O'Leary, R. Witzgall, M. Vidal, J. V. Bonventre, A novel
1004 member of the RING finger family, KRIP-1, associates with the KRAB-A transcriptional
1005 repressor domain of zinc finger proteins. *Proc Natl Acad Sci U S A* **93**, 15299-15304
1006 (1996).
1007 21. L. Lionnard, P. Duc, M. S. Brennan, A. J. Kueh, M. Pal, F. Guardia, B. Mojsa, M. A.
1008 Damiano, S. Mora, I. Lassot, R. Ravichandran, C. Cochet, A. Aouacheria, P. R. Potts, M.
1009 J. Herold, S. Desagher, J. Kucharczak, TRIM17 and TRIM28 antagonistically regulate the
1010 ubiquitination and anti-apoptotic activity of BCL2A1. *Cell Death Differ* **26**, 902-917
1011 (2019).
1012 22. W. J. Kim, B. S. Wittner, A. Amzallag, B. W. Brannigan, D. T. Ting, S. Ramaswamy, S.
1013 Maheswaran, D. A. Haber, The WTX Tumor Suppressor Interacts with the Transcriptional
1014 Corepressor TRIM28. *J Biol Chem* **290**, 14381-14390 (2015).
1015 23. K. Singh, M. Cassano, E. Planet, S. Sebastian, S. M. Jang, G. Sohi, H. Faralli, J. Choi, H.
1016 D. Youn, F. J. Dilworth, D. Trono, A KAP1 phosphorylation switch controls MyoD
1017 function during skeletal muscle differentiation. *Genes Dev* **29**, 513-525 (2015).
1018 24. F. Cammas, M. Mark, P. Dolle, A. Dierich, P. Chambon, R. Losson, Mice lacking the
1019 transcriptional corepressor TIF1beta are defective in early postimplantation development.
1020 *Development* **127**, 2955-2963 (2000).
1021 25. N. D. Steinert, G. K. Potts, G. M. Wilson, A. M. Klamen, K. H. Lin, J. B. Hermanson, R.
1022 M. McNally, J. J. Coon, T. A. Hornberger, Mapping of the contraction-induced
1023 phosphoproteome identifies TRIM28 as a significant regulator of skeletal muscle size and
1024 function. *Cell Rep* **34**, 108796 (2021).
1025 26. G. K. Potts, R. M. McNally, R. Blanco, J. S. You, A. S. Hebert, M. S. Westphall, J. J.
1026 Coon, T. A. Hornberger, A map of the phosphoproteomic alterations that occur after a
1027 bout of maximal-intensity contractions. *J Physiol* **595**, 5209-5226 (2017).

1028 27. M. M. Murphy, J. A. Lawson, S. J. Mathew, D. A. Hutcheson, G. Kardon, Satellite cells,
1029 connective tissue fibroblasts and their interactions are crucial for muscle regeneration.
1030 *Development* **138**, 3625-3637 (2011).
1031 28. X. Sun, A. Bizhanova, T. D. Matheson, J. Yu, L. J. Zhu, P. D. Kaufman, Ki-67
1032 Contributes to Normal Cell Cycle Progression and Inactive X Heterochromatin in p21
1033 Checkpoint-Proficient Human Cells. *Mol Cell Biol* **37**, (2017).
1034 29. J. Gerdes, U. Schwab, H. Lemke, H. Stein, Production of a mouse monoclonal antibody
1035 reactive with a human nuclear antigen associated with cell proliferation. *Int J Cancer* **31**,
1036 13-20 (1983).
1037 30. V. Randrianarison-Huetz, A. Papaefthymiou, G. Herledan, C. Noviello, U. Faradova, L.
1038 Collard, A. Pincini, E. Schol, J. F. Decaux, P. Maire, S. Vassilopoulos, A. Sotiropoulos,
1039 Srf controls satellite cell fusion through the maintenance of actin architecture. *J Cell Biol*
1040 **217**, 685-700 (2018).
1041 31. H. K. Smith, L. Maxwell, C. D. Rodgers, N. H. McKee, M. J. Plyley, Exercise-enhanced
1042 satellite cell proliferation and new myonuclear accretion in rat skeletal muscle. *J Appl*
1043 *Physiol (1985)* **90**, 1407-1414 (2001).
1044 32. J. K. Petrella, J. S. Kim, D. L. Mayhew, J. M. Cross, M. M. Bamman, Potent myofiber
1045 hypertrophy during resistance training in humans is associated with satellite cell-mediated
1046 myonuclear addition: a cluster analysis. *J Appl Physiol (1985)* **104**, 1736-1742 (2008).
1047 33. A. K. Borowik, A. Davidyan, F. F. Peelor, 3rd, E. Voloviceva, S. M. Doidge, M. P.
1048 Bubak, C. B. Mobley, J. J. McCarthy, E. E. Dupont-Versteegden, B. F. Miller, Skeletal
1049 Muscle Nuclei in Mice are not Post-mitotic. *Function (Oxf)* **4**, zqac059 (2023).
1050 34. W. E. Pullman, G. C. Yeoh, The role of myonuclei in muscle regeneration: an in vitro
1051 study. *J Cell Physiol* **96**, 245-251 (1978).
1052 35. Q. Goh, D. P. Millay, Requirement of myomaker-mediated stem cell fusion for skeletal
1053 muscle hypertrophy. *Elife* **6**, (2017).
1054 36. Q. Goh, T. Song, M. J. Petrany, A. A. Cramer, C. Sun, S. Sadayappan, S. J. Lee, D. P.
1055 Millay, Myonuclear accretion is a determinant of exercise-induced remodeling in skeletal
1056 muscle. *Elife* **8**, (2019).
1057 37. A. Guerci, C. Lahoute, S. Hebrard, L. Collard, D. Graindorge, M. Favier, N. Cagnard, S.
1058 Batonnet-Pichon, G. Precigout, L. Garcia, D. Tuil, D. Daegelen, A. Sotiropoulos, Srf-
1059 dependent paracrine signals produced by myofibers control satellite cell-mediated skeletal
1060 muscle hypertrophy. *Cell Metab* **15**, 25-37 (2012).
1061 38. D. Selcen, K. Ohno, A. G. Engel, Myofibrillar myopathy: clinical, morphological and
1062 genetic studies in 63 patients. *Brain : a journal of neurology* **127**, 439-451 (2004).
1063 39. J. J. McCarthy, J. Mula, M. Miyazaki, R. Erfani, K. Garrison, A. B. Farooqui, R. Srikuea,
1064 B. A. Lawson, B. Grimes, C. Keller, G. Van Zant, K. S. Campbell, K. A. Esser, E. E.
1065 Dupont-Versteegden, C. A. Peterson, Effective fiber hypertrophy in satellite cell-depleted
1066 skeletal muscle. *Development* **138**, 3657-3666 (2011).
1067 40. C. Lepper, T. A. Partridge, C. M. Fan, An absolute requirement for Pax7-positive satellite
1068 cells in acute injury-induced skeletal muscle regeneration. *Development* **138**, 3639-3646
1069 (2011).
1070 41. R. Sambasivan, R. Yao, A. Kissenpfennig, L. Van Wittenberghe, A. Paldi, B. Gayraud-
1071 Morel, H. Guenou, B. Malissen, S. Tajbakhsh, A. Galy, Pax7-expressing satellite cells are
1072 indispensable for adult skeletal muscle regeneration. *Development* **138**, 3647-3656 (2011).
1073 42. A. B. Morton, C. E. Norton, N. L. Jacobsen, C. A. Fernando, D. D. W. Cornelison, S. S.
1074 Segal, Barium chloride injures myofibers through calcium-induced proteolysis with
1075 fragmentation of motor nerves and microvessels. *Skeletal muscle* **9**, 27 (2019).

1076 43. S. Guiraud, B. Edwards, S. E. Squire, L. Moir, A. Berg, A. Babbs, N. Ramadan, M. J.
1077 Wood, K. E. Davies, Embryonic myosin is a regeneration marker to monitor utrophin-
1078 based therapies for DMD. *Human molecular genetics* **28**, 307-319 (2019).
1079 44. S. Schiaffino, L. Gorza, S. Sartore, L. Saggin, M. Carli, Embryonic myosin heavy chain as
1080 a differentiation marker of developing human skeletal muscle and rhabdomyosarcoma. A
1081 monoclonal antibody study. *Exp Cell Res* **163**, 211-220 (1986).
1082 45. D. P. Millay, Regulation of the myoblast fusion reaction for muscle development,
1083 regeneration, and adaptations. *Exp Cell Res* **415**, 113134 (2022).
1084 46. R. Duan, P. J. Gallagher, Dependence of myoblast fusion on a cortical actin wall and
1085 nonmuscle myosin IIA. *Developmental biology* **325**, 374-385 (2009).
1086 47. R. Duan, J. H. Kim, K. Shilagardi, E. S. Schiffhauer, D. M. Lee, S. Son, S. Li, C. Thomas,
1087 T. Luo, D. A. Fletcher, D. N. Robinson, E. H. Chen, Spectrin is a mechanoresponsive
1088 protein shaping fusogenic synapse architecture during myoblast fusion. *Nat Cell Biol* **20**,
1089 688-698 (2018).
1090 48. P. Bi, J. R. McAnally, J. M. Shelton, E. Sanchez-Ortiz, R. Bassel-Duby, E. N. Olson,
1091 Fusogenic micropeptide Myomixer is essential for satellite cell fusion and muscle
1092 regeneration. *Proc Natl Acad Sci U S A* **115**, 3864-3869 (2018).
1093 49. D. P. Millay, L. B. Sutherland, R. Bassel-Duby, E. N. Olson, Myomaker is essential for
1094 muscle regeneration. *Genes Dev* **28**, 1641-1646 (2014).
1095 50. H. K. Sihvo, K. Immonen, E. Puolanne, Myodegeneration with fibrosis and regeneration
1096 in the pectoralis major muscle of broilers. *Vet Pathol* **51**, 619-623 (2014).
1097 51. C. J. Mann, E. Perdiguero, Y. Kharraz, S. Aguilar, P. Pessina, A. L. Serrano, P. Munoz-
1098 Canoves, Aberrant repair and fibrosis development in skeletal muscle. *Skeletal muscle* **1**,
1099 21 (2011).
1100 52. C. S. Fry, T. J. Kirby, K. Kosmac, J. J. McCarthy, C. A. Peterson, Myogenic Progenitor
1101 Cells Control Extracellular Matrix Production by Fibroblasts during Skeletal Muscle
1102 Hypertrophy. *Cell stem cell* **20**, 56-69 (2017).
1103 53. D. R. Lemos, F. Babaeijandaghi, M. Low, C. K. Chang, S. T. Lee, D. Fiore, R. H. Zhang,
1104 A. Natarajan, S. A. Nedospasov, F. M. Rossi, Nilotinib reduces muscle fibrosis in chronic
1105 muscle injury by promoting TNF-mediated apoptosis of fibro/adipogenic progenitors. *Nat*
1106 *Med* **21**, 786-794 (2015).
1107 54. R. Y. Chen-Tsai, Using TARGATT Technology to Generate Site-Specific Transgenic
1108 Mice. *Methods Mol Biol* **1874**, 71-86 (2019).
1109 55. E. Leikina, D. G. Gamage, V. Prasad, J. Goykhberg, M. Crowe, J. Diao, M. M. Kozlov, L.
1110 V. Chernomordik, D. P. Millay, Myomaker and Myomerger Work Independently to
1111 Control Distinct Steps of Membrane Remodeling during Myoblast Fusion. *Developmental*
1112 *cell* **46**, 767-780 e767 (2018).
1113 56. L. V. Chernomordik, M. M. Kozlov, Membrane hemifusion: crossing a chasm in two
1114 leaps. *Cell* **123**, 375-382 (2005).
1115 57. G. Golani, E. Leikina, K. Melikov, J. M. Whitlock, D. G. Gamage, G. Luoma-Overstreet,
1116 D. P. Millay, M. M. Kozlov, L. V. Chernomordik, Myomerger promotes fusion pore by
1117 elastic coupling between proximal membrane leaflets and hemifusion diaphragm. *Nature*
1118 *communications* **12**, 495 (2021).
1119 58. D. P. Millay, J. R. O'Rourke, L. B. Sutherland, S. Bezprozvannaya, J. M. Shelton, R.
1120 Bassel-Duby, E. N. Olson, Myomaker is a membrane activator of myoblast fusion and
1121 muscle formation. *Nature* **499**, 301-305 (2013).
1122 59. P. Bi, A. Ramirez-Martinez, H. Li, J. Cannavino, J. R. McAnally, J. M. Shelton, E.
1123 Sanchez-Ortiz, R. Bassel-Duby, E. N. Olson, Control of muscle formation by the
1124 fusogenic micropeptide myomixer. *Science* **356**, 323-327 (2017).

1125 60. Q. Zhang, A. A. Vashisht, J. O'Rourke, S. Y. Corbel, R. Moran, A. Romero, L. Miraglia,
1126 J. Zhang, E. Durrant, C. Schmedt, S. C. Sampath, S. C. Sampath, The microprotein
1127 Minion controls cell fusion and muscle formation. *Nature communications* **8**, 15664
1128 (2017).
1129 61. M. E. Quinn, Q. Goh, M. Kurosaka, D. G. Gamage, M. J. Petrany, V. Prasad, D. P. Millay,
1130 Myomerger induces fusion of non-fusogenic cells and is required for skeletal muscle
1131 development. *Nature communications* **8**, 15665 (2017).
1132 62. H. Zhang, J. Wen, A. Bigot, J. Chen, R. Shang, V. Mouly, P. Bi, Human myotube
1133 formation is determined by MyoD-Myomixer/Myomaker axis. *Sci Adv* **6**, (2020).
1134 63. A. Musarò, The Basis of Muscle Regeneration. *Advances in Biology* **2014**, 612471 (2014).
1135 64. S. E. Iismaa, X. Kaidonis, A. M. Nicks, N. Bogush, K. Kikuchi, N. Naqvi, R. P. Harvey,
1136 A. Husain, R. M. Graham, Comparative regenerative mechanisms across different
1137 mammalian tissues. *NPJ Regen Med* **3**, 6 (2018).
1138 65. N. Yanay, M. Rabie, Y. Nevo, Impaired Regeneration in Dystrophic Muscle-New Target
1139 for Therapy. *Front Mol Neurosci* **13**, 69 (2020).
1140 66. P. Munoz-Canoves, J. Neves, P. Sousa-Victor, Understanding muscle regenerative decline
1141 with aging: new approaches to bring back youthfulness to aged stem cells. *The FEBS*
1142 *journal* **287**, 406-416 (2020).
1143 67. L. Fasching, A. Kapopoulou, R. Sachdeva, R. Petri, M. E. Jonsson, C. Manne, P. Turelli,
1144 P. Jern, F. Cammas, D. Trono, J. Jakobsson, TRIM28 represses transcription of
1145 endogenous retroviruses in neural progenitor cells. *Cell Rep* **10**, 20-28 (2015).
1146 68. H. M. Rowe, J. Jakobsson, D. Mesnard, J. Rougemont, S. Reynard, T. Aktas, P. V.
1147 Maillard, H. Layard-Liesching, S. Verp, J. Marquis, F. Spitz, D. B. Constam, D. Trono,
1148 KAP1 controls endogenous retroviruses in embryonic stem cells. *Nature* **463**, 237-240
1149 (2010).
1150 69. M. C. Milone, U. O'Doherty, Clinical use of lentiviral vectors. *Leukemia* **32**, 1529-1541
1151 (2018).
1152 70. J. Saha, J. Bae, S. Y. Wang, H. Lu, L. J. Chappell, P. Gopal, A. J. Davis, Ablating putative
1153 Ku70 phosphorylation sites results in defective DNA damage repair and spontaneous
1154 induction of hepatocellular carcinoma. *Nucleic acids research* **49**, 9836-9850 (2021).
1155 71. I. Ruvinsky, N. Sharon, T. Lerer, H. Cohen, M. Stolovich-Rain, T. Nir, Y. Dor, P. Zisman,
1156 O. Meyuhas, Ribosomal protein S6 phosphorylation is a determinant of cell size and
1157 glucose homeostasis. *Genes Dev* **19**, 2199-2211 (2005).
1158 72. P. C. Witcher, C. Sun, D. P. Millay, Expression of Myomaker and Myomerger in
1159 myofibers causes muscle pathology. *Skeletal muscle* **13**, 8 (2023).
1160 73. C. T. Cheng, C. Y. Kuo, D. K. Ann, KAPtain in charge of multiple missions: Emerging
1161 roles of KAP1. *World J Biol Chem* **5**, 308-320 (2014).
1162 74. M. W. Rousseaux, M. de Haro, C. A. Lasagna-Reeves, A. De Maio, J. Park, P. Jafar-
1163 Nejad, I. Al-Ramahi, A. Sharma, L. See, N. Lu, L. Vilanova-Velez, T. J. Klisch, T. F.
1164 Westbrook, J. C. Troncoso, J. Botas, H. Y. Zoghbi, TRIM28 regulates the nuclear
1165 accumulation and toxicity of both alpha-synuclein and tau. *Elife* **5**, (2016).
1166 75. J. O. Jin, G. D. Lee, S. H. Nam, T. H. Lee, D. H. Kang, J. K. Yun, P. C. Lee, Sequential
1167 ubiquitination of p53 by TRIM28, RLIM, and MDM2 in lung tumorigenesis. *Cell Death*
1168 *Differ* **28**, 1790-1803 (2021).
1169 76. D. Komander, The emerging complexity of protein ubiquitination. *Biochem Soc Trans* **37**,
1170 937-953 (2009).
1171 77. B. Sehat, A. Tofigh, Y. Lin, E. Trocme, U. Liljedahl, J. Lagergren, O. Larsson,
1172 SUMOylation mediates the nuclear translocation and signaling of the IGF-1 receptor.
1173 *Science signaling* **3**, ra10 (2010).

78. J. S. You, R. M. McNally, B. L. Jacobs, R. E. Privett, D. M. Gundermann, K. H. Lin, N. D. Steinert, C. A. Goodman, T. A. Hornberger, The role of raptor in the mechanical load-induced regulation of mTOR signaling, protein synthesis, and skeletal muscle hypertrophy. *FASEB J* **33**, 4021-4034 (2019).
79. C. A. Goodman, J. W. Frey, D. M. Mabrey, B. L. Jacobs, H. C. Lincoln, J. S. You, T. A. Hornberger, The role of skeletal muscle mTOR in the regulation of mechanical load-induced growth. *J Physiol* **589**, 5485-5501 (2011).
80. L. Hindi, J. D. McMillan, D. Afroze, S. M. Hindi, A. Kumar, Isolation, Culturing, and Differentiation of Primary Myoblasts from Skeletal Muscle of Adult Mice. *Bio Protoc* **7**, (2017).

Acknowledgments

We would like to thank Drs. Marco Cassano and Didier Trono for providing plasmids that were used for lentiviral production. We also would like to thank Dr. Dustin Rubinstein and Kathy Krentz at the Genome Editing and Animal Models Facility (University of Wisconsin-Madison) for their assistance with the generation of the knockin mice.

Funding:
The research reported in this publication was supported by the National Institute of Arthritis and Musculoskeletal and Skin Diseases of the National Institutes of Health under Awards AR074932 to TAH, AR074932-S1 to TAH and JEH, and P30AR066524 to VS.

Author contributions:

Conceptualization: KHL, JEH, NDS, TAH
Methodology: KHL, JEH, NDS, TAH
Formal analysis: KHL, JEH, TAH
Investigation: KHL, JEH, JLL, MMT, NDS, PMF, KMM, ML, VS, TAH
Visualization: KHL, JEH, TAH
Supervision: TAH
Writing—original draft: KHL, JEH, TAH
Writing—review & editing: KHL, JEH, JLL, MMT, PMF, KMM, JFD, TAH
Funding acquisition: JEH, TAH

Competing interests: Authors declare that they have no competing interests.

Data and materials availability: All data generated and materials used and/or analyzed during the current study are available from the corresponding author upon reasonable request.

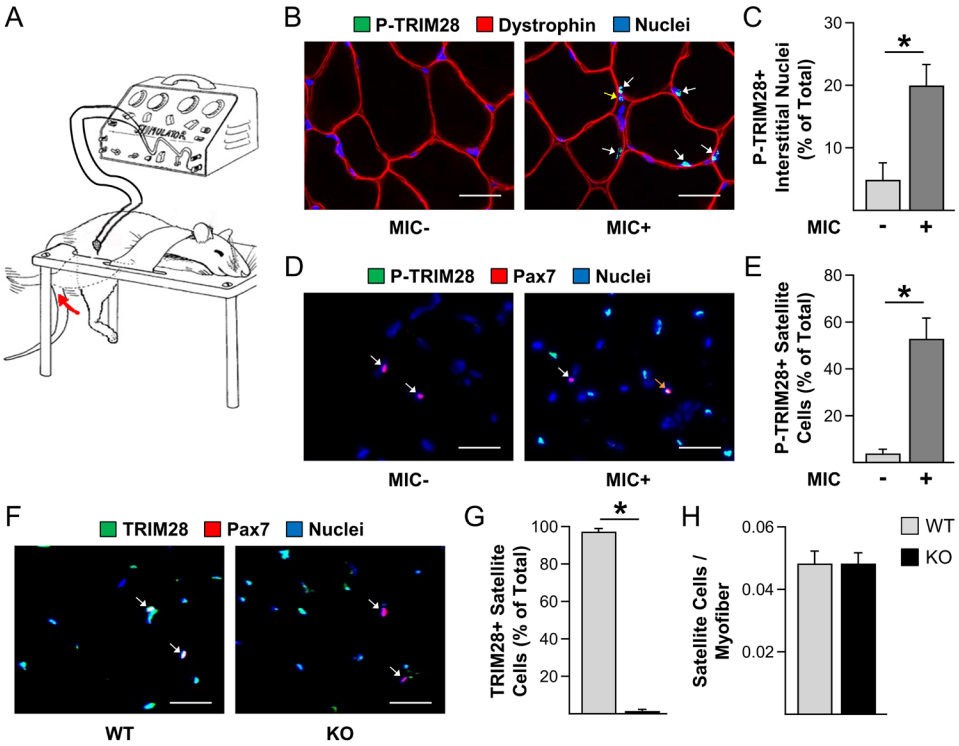

Fig. 1. Maximal intensity contractions induce TRIM28(S473) phosphorylation in satellite cells. (**A**) Tibialis anterior muscles of male wild-type (WT) mice were subjected to a bout of maximal-intensity contractions (MIC+) or the control condition (MIC-) and collected at 1 hour post-treatment. (**B**) Mid-belly cross-sections of the tibialis anterior muscles were subjected to immunohistochemistry for phosphorylated (P) TRIM28(S473), dystrophin (to identify the outer boundary of the myofibers), and nuclei. White arrows indicate P-TRIM28 positive myonuclei and yellow arrows indicate P-TRIM28 positive interstitial nuclei. (**C**) Quantification of the % of P-TRIM28(S473) positive (+) interstitial nuclei from B. (**D**) Mid-belly cross-sections of MIC- and MIC+ tibialis anterior muscles were subjected to immunohistochemistry for P-TRIM28(S473), Pax7 (to identify satellite cells), and nuclei. White arrows indicate P-TRIM28 negative satellite cells and the orange arrow indicates a P-TRIM28 positive satellite cell. (**E**) Images in D were used to quantify the percentage of satellite cells that were P-TRIM28(S473) positive. (**F**) WT mice and tamoxifen-inducible satellite cell-specific TRIM28 knockout mice (KO) were treated with tamoxifen. At 14 days post tamoxifen, mid-belly cross-sections from the plantaris muscle were subjected to immunohistochemistry for TRIM28, Pax7, and nuclei. White arrows indicate satellite cells. (**G-H**) Quantification of the percentage of satellite cells that were TRIM28 positive (G) and the satellite cell to myofiber ratio (H). All values are group means + SEM, n = 3-4/group. Data were analyzed with Student's t-tests. * indicates a significant difference between groups, $p < 0.05$. Scale bars = 25 µm.

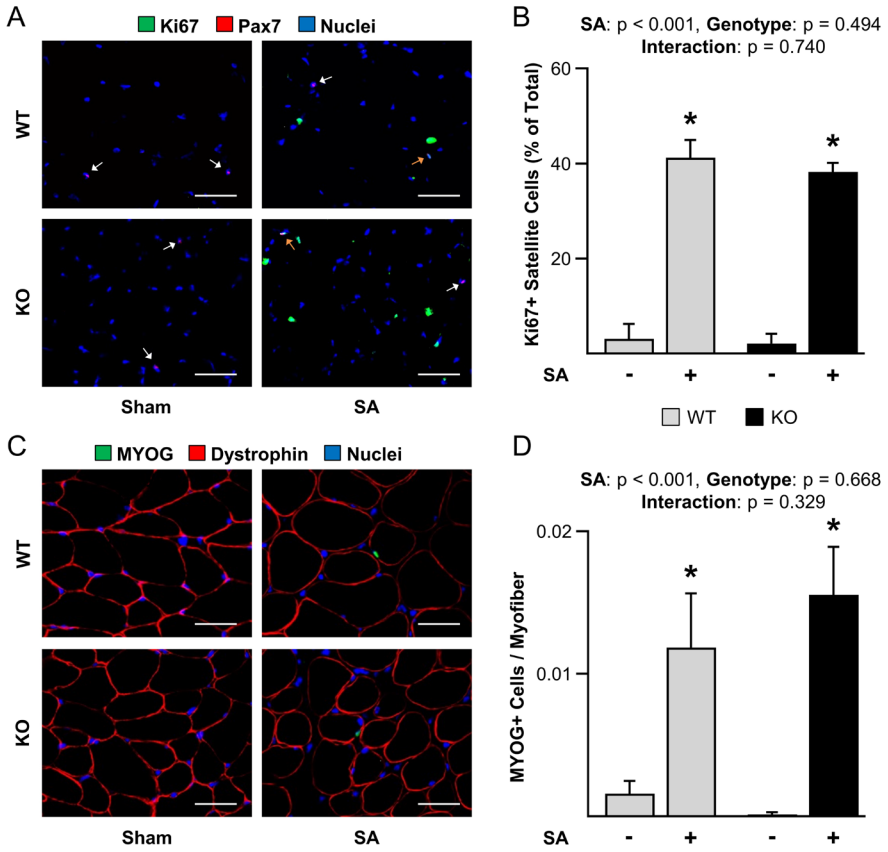

Fig. 2. The loss of TRIM28 does not alter the mechanical load-induced proliferation or differentiation of satellite cells. Wild-type (WT) mice and tamoxifen-inducible satellite cell-specific TRIM28 knockout mice (KO) were treated with tamoxifen. At 14 days post tamoxifen, the plantaris muscles of mice were subjected to a unilateral synergist ablation surgery (SA+), with the non-ablated limb serving as a sham control (SA-). The plantaris muscles were collected 4 days post-surgery and subjected to the following analyses. (**A**) Mid-belly cross-sections were subjected to immunohistochemistry for Pax7, Ki67 (a marker of proliferating cells), and nuclei. White arrows indicate Ki67 negative satellite cells and orange arrows indicate Ki67 positive satellite cells. (**B**) Quantification of the percentage of satellite cells in A that were Ki67 positive. (**C**) Mid-belly cross-sections were subjected to immunohistochemistry for MYOG (a marker of differentiated satellite cells), dystrophin, and nuclei. (**D**) Quantification of the MYOG positive cell to myofiber ratio in C. Values are means + SEM, n = 4-8/group. Data were analyzed with two-way ANOVA. * indicates a significant effect of SA within the given genotype, $p < 0.05$. Scale bars = 50 µm.

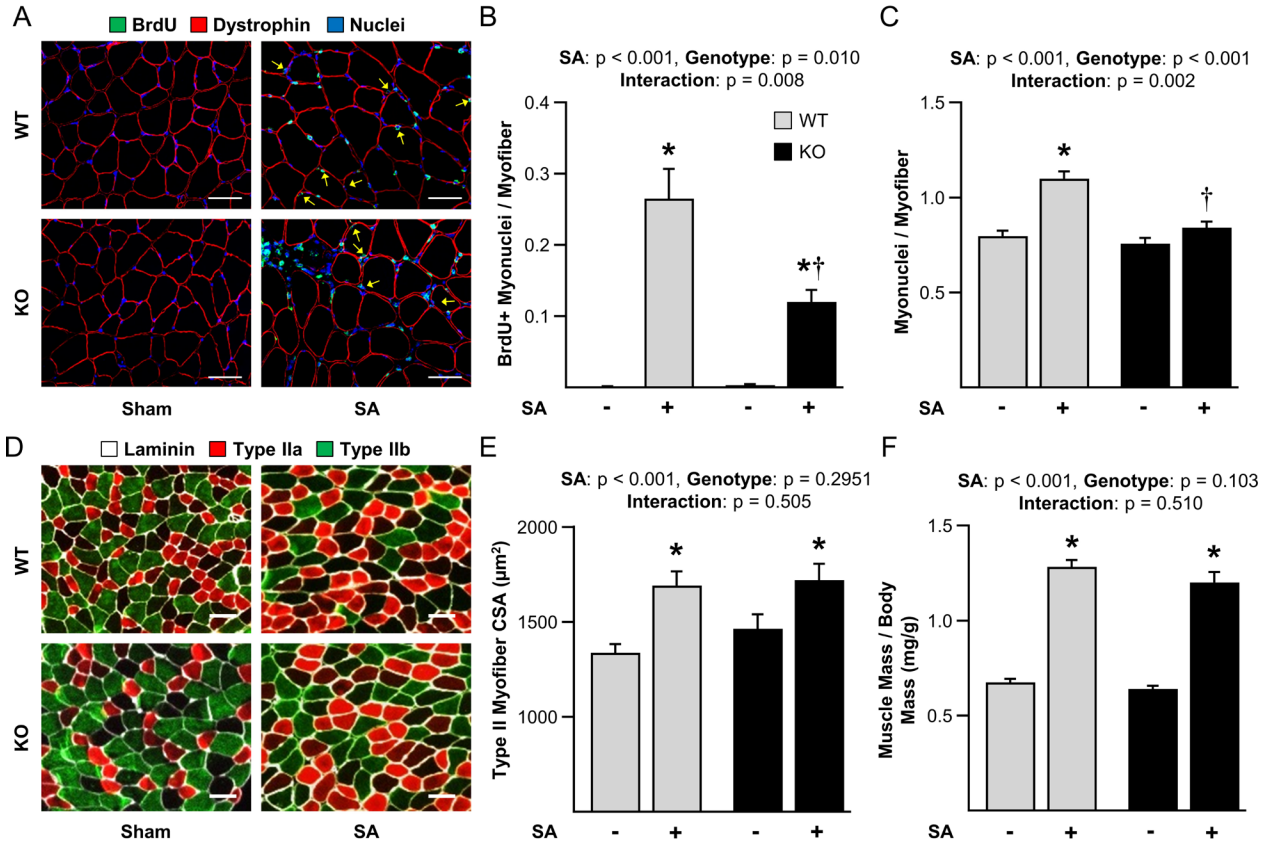

Fig. 3. The loss of TRIM28 in satellite cells attenuates mechanical load-induced myonuclear accretion but it does not alter the increase in muscle mass or myofiber size. Wild-type (WT) mice and tamoxifen-inducible satellite cell-specific TRIM28 knockout mice (KO) were treated with tamoxifen. At 14 days post tamoxifen, mice were subjected to unilateral synergist ablation surgery (SA+), with the non-ablated limb serving as a sham control (SA-). The mice were given daily intraperitoneal injections of BrdU for 14 days to label cells with replicated DNA and then the plantaris muscles were collected. (**A**) Mid-belly cross-sections were subjected to immunohistochemistry for BrdU, dystrophin, and nuclei. Yellow arrows indicate BrdU-positive myonuclei. (**B**) Quantification of the BrdU positive myonuclei to myofiber ratio and (**C**) the total myonuclei to myofiber ratio in A. (**D**) Mid-belly cross-sections were subjected to immunohistochemistry for laminin and the identification of myofiber type. (**E**) The average CSA of the type IIa, IIx, and IIb myofibers was determined and reported as type II myofiber CSA. (**F**) The muscle mass to body mass ratio. Note: half of the mice in E and F were BrdU injected and the other half were not. No difference between the conditions was observed (data not shown). Values are group means + SEM, n = 6-12/group. Data were analyzed with two-way ANOVA. * indicates a significant effect of SA within the given genotype, † indicates a significant difference between the SA groups, $p < 0.05$. Scale bars = 50 μm.

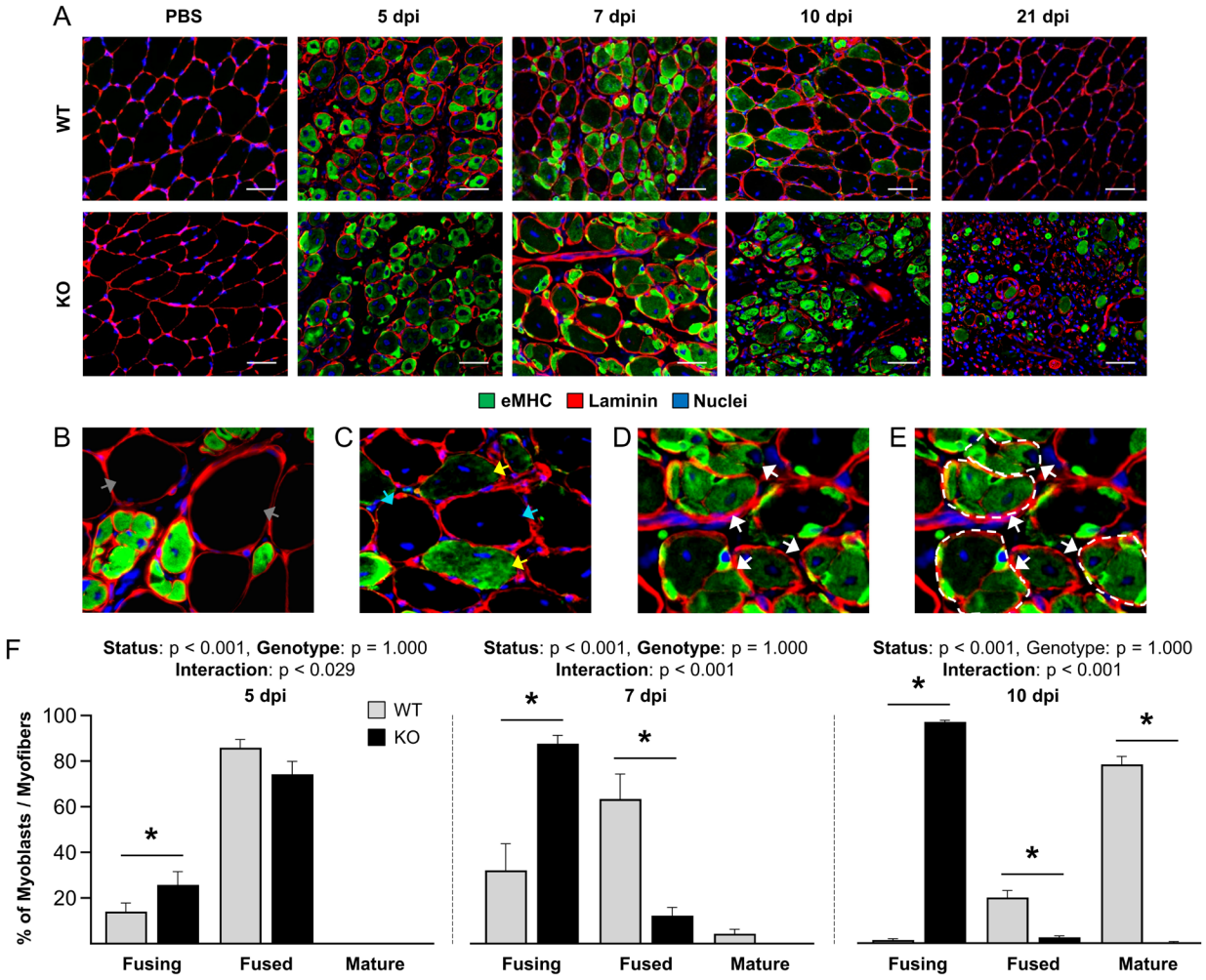

Fig. 4. The loss of TRIM28 in satellite cells leads to impaired fusion during injury-induced myogenesis/regeneration. Wild-type (WT) mice and tamoxifen-inducible satellite cell-specific TRIM28 knockout mice (KO) mice were treated with tamoxifen. At 14 days post tamoxifen, their tibialis anterior muscles were injected with $BaCl_2$ to induce injury or PBS as a control condition. (**A**) At 5, 7, 10, and 21 days post-injury (dpi), tibialis anterior muscles were collected and mid-belly cross-sections were subjected to immunohistochemistry for eMHC, laminin, and nuclei. (**B-E**) The myoblasts/myofibers in A were categorized as being in one of the following stages: fusing, fused, mature, or pre-existing. (B) Pre-existing (gray arrows) were defined as eMHC negative myofibers that did not contain centrally located nuclei and were likely not damaged by $BaCl_2$. (C) Mature (cyan arrows) were defined as eMHC-negative myofibers with centrally located nuclei. Fused (yellow arrows) were defined as eMHC-positive myoblasts/myofibers that did not contain interior laminin borders. (D-E) Fusing (white arrows) were defined as myoblasts/myofibers that contained clusters of eMHC positive cells that possessed individual laminin borders and were surrounded by a thicker outer laminin border (white dashed line in E). (**F**) Proportion of myoblasts/myofibers at 5, 7, and 10 dpi that were at the stage of fusing, fused, or mature. Values are means + SEM, n = 4-6/group. Data were analyzed with two-way ANOVA. * indicates a significant difference from WT within the same category of myoblasts/myofibers. $p < 0.05$. Scale bars = 50 μm.

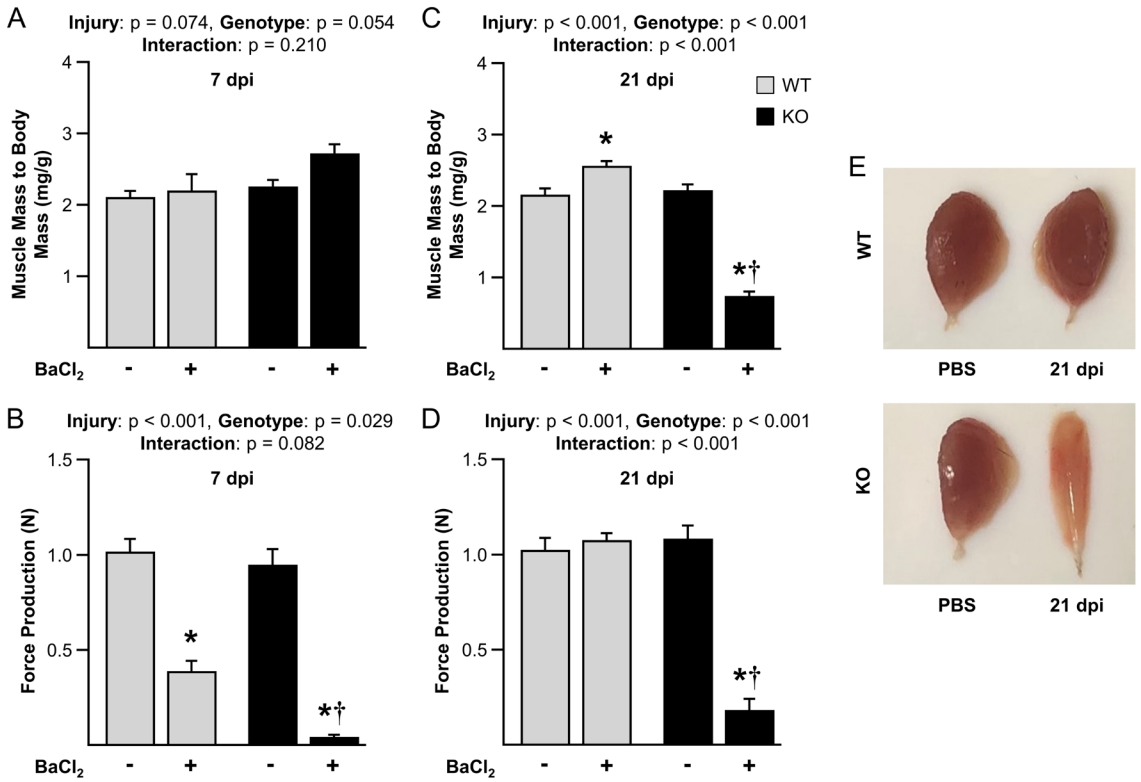

Fig. 5. The loss of TRIM28 in satellite cells leads to a profound functional deficit following $BaCl_2$-induced injury. Wild-type (WT) mice and tamoxifen-inducible satellite cell-specific TRIM28 knockout mice (KO) mice were treated with tamoxifen. At 14 days post tamoxifen, their tibialis anterior muscles were injected with $BaCl_2$ (+) to induce injury or PBS (-) as a control condition. At 7 days post-injury (dpi), (**A**) the muscle mass to body mass ratio and (**B**) *in situ* peak tetanic force production were measured. At 21 dpi, (**C**) the muscle mass to body mass ratio and (**D**) *in situ* peak tetanic force production were measured. (**E**) The gross appearance of tibialis anterior muscles at 21 dpi. Values are group means + SEM, n = 4-6/group. Data were analyzed with two-way repeated-measures ANOVA. * indicates a significant effect of injury, † indicates a significant difference between the $BaCl_2$ treated groups, $p < 0.05$.

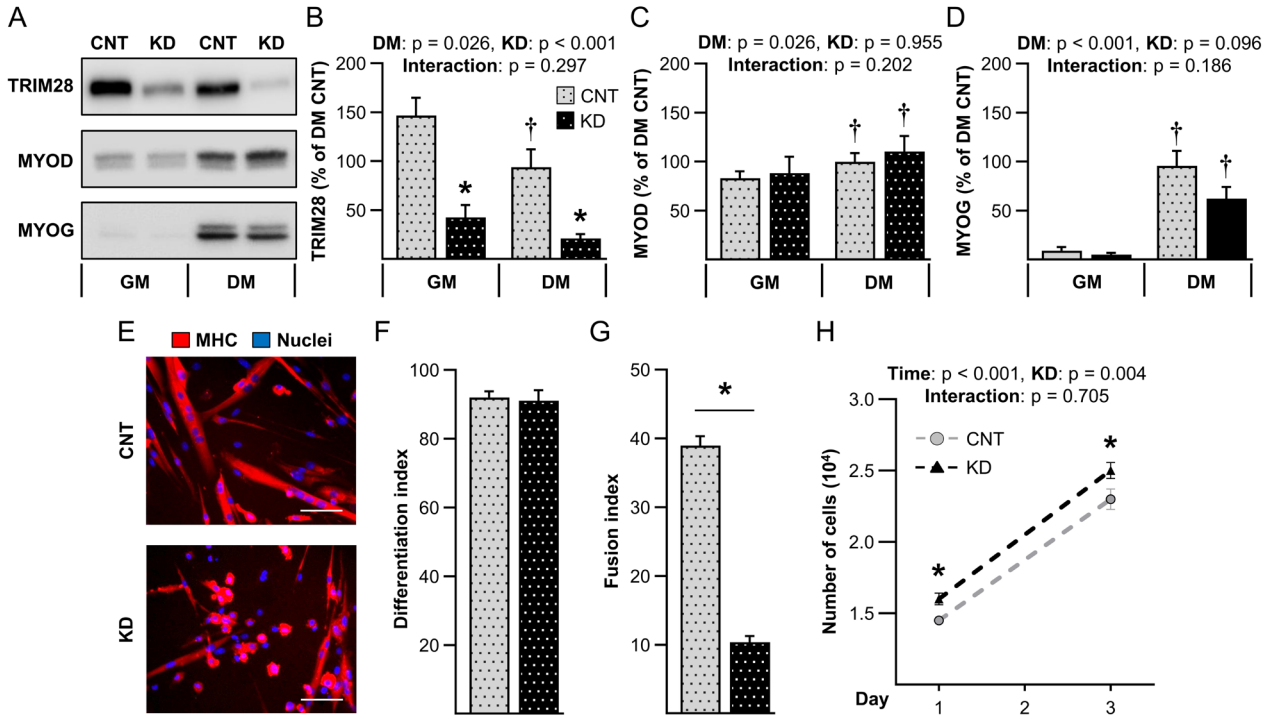

Fig. 6. Knockdown of TRIM28 leads to a fusion defect during *in vitro* myotube formation (**A-D**) Primary myoblasts were infected with lentivirus expressing scrambled shRNA (CNT) or shRNA targeting Trim28 mRNA (KD). The infected cells were cultured in growth media (GM) or differentiation media (DM) for 2 days and subjected to western blot analysis (WB) of TRIM28, MYOD, and MYOG. (**E-G**) Infected myoblasts were subjected to a myotube formation assay and immunohistochemistry for MHC and nuclei. (F) The differentiation index (% of nuclei inside MHC positive cells), and (G) the fusion index (% of nuclei inside MHC positive multinucleated cells) were quantified. (**H**) $2x10^4$ infected myoblasts were seeded on day 0 and quantified on days 1 and 3. Values are group means + SEM, n = 4/group with each sample representing an independent line of isolated primary myoblasts. Data in B-D and H were analyzed with two-way repeated-measures ANOVA, whereas F and G were analyzed with Student's t-tests. * indicates a significant effect of genotype within a given condition, † significant effect of DM within a given genotype, $p < 0.05$. Scale bars = 50 µm.

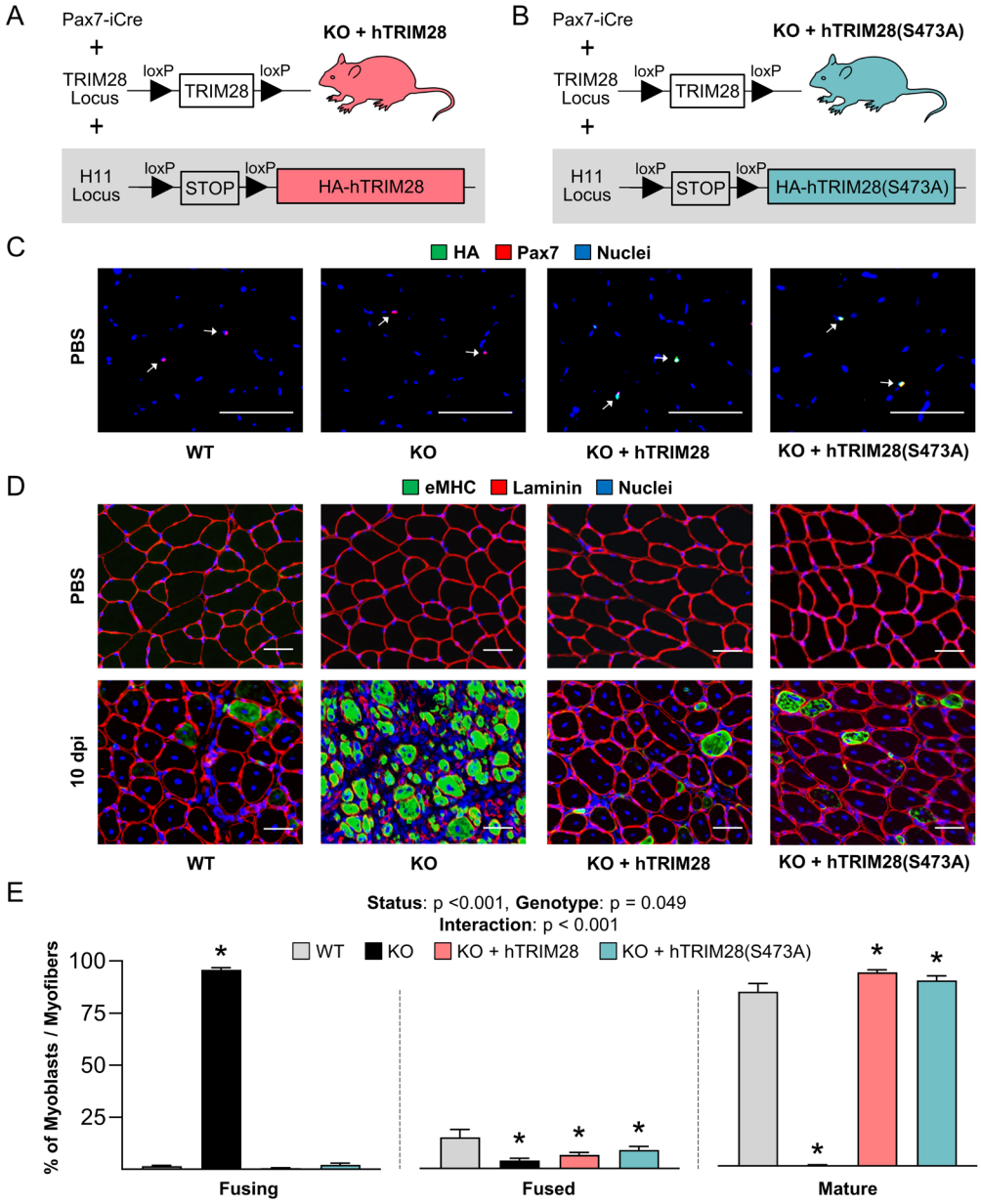

Fig. 7. TRIM28(S473) phosphorylation in satellite cells is not required for injury-induced fusion *in vivo*. Strategy for creating mice that allowed for tamoxifen-inducible and satellite cell-specific knockout of endogenous TRIM28 along with tamoxifen-inducible and satellite cell-specific "rescue" expression of (**A**) human TRIM28 (KO + hTRIM28) or (**B**) a S473A phosphodefective mutant of hTRIM28 (KO + hTRIM28(S473A)). (**C**) Wild-type (WT), tamoxifen-inducible satellite cell-specific TRIM28 knockout (KO), KO + hTRIM28, and KO + hTRIM28(S473A) mice were treated with tamoxifen. At 14 days post-tamoxifen, mid-belly cross sections from the tibialis anterior muscles were subjected to immunohistochemistry for Pax7, HA, and nuclei. White arrows indicate satellite cells. (**D**) At 14 days post tamoxifen tibialis anterior muscles were injected with $BaCl_2$ to induce injury or PBS as a control condition. At 10 days post-injury (dpi), mid-belly cross sections of the tibialis anterior muscles were subjected to immunohistochemistry for eMHC, laminin, and nuclei. As defined in Fig. 4, myoblasts/myofibers in the injured muscles were assigned to one of the following four stages: fusing, fused, mature, or pre-existing. (**E**) Proportion of myoblasts/myofibers that were at the stage of fusing, fused, or mature. Values are presented as the group mean + SEM, $n = 6$/group. Data were analyzed with two-way repeated-measures ANOVA. * indicates a significant difference from WT, $p < 0.05$. Scale bars = 50 µm.

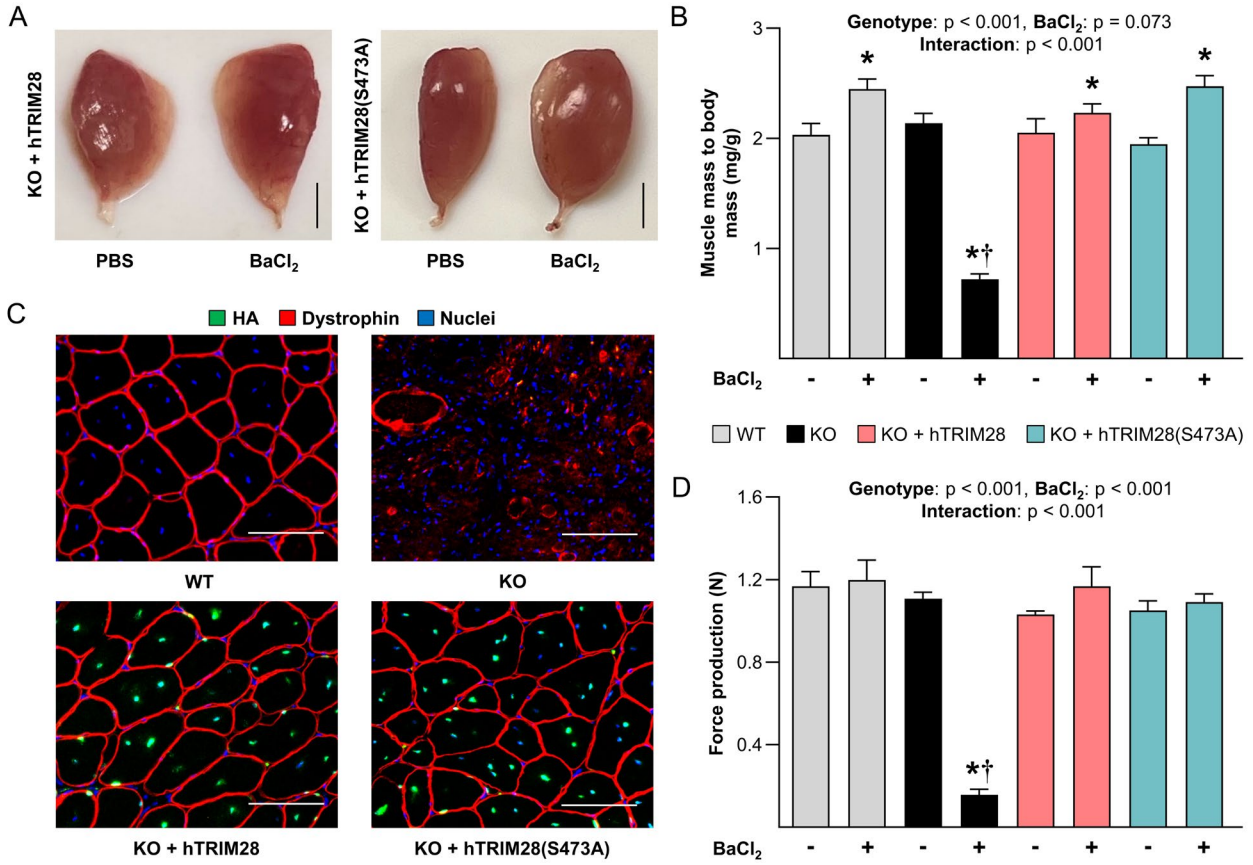

Fig. 8. TRIM28(S473) phosphorylation in satellite cells is not required for injury-induced myogenesis/regeneration. At 14 days post tamoxifen the tibialis anterior muscles of wild-type (WT) mice, tamoxifen-inducible and satellite cell-specific TRIM28 knockout mice (KO) mice, as well as KO mice that contain tamoxifen-inducible "rescue" expression of hTRIM28 (KO + hTRIM28) or phosphodefective hTRIM28 (KO + hTRIM28(S473A)) were injected with $BaCl_2$ (+) to induce injury or PBS (-) as a control condition. The tibialis anterior muscles were collected at 21 days post-injury. (**A**) Gross appearance of tibialis anterior muscles. Scale bars = 2 mm (see Fig. 5 for representative images of the WT and KO muscles). (**B**) The muscle mass to body mass ratios. (**C**) Mid-belly cross sections of the muscles were subjected to immunohistochemistry for the HA tag, dystrophin, and nuclei. Scale bars = 50 µm. (**D**) *In situ* peak tetanic force production. Values are presented as the group mean + SEM, n = 6-9/group. The data were analyzed with two-way repeated-measures ANOVA. * indicates a significant effect of $BaCl_2$ within a given genotype, † indicates significant difference from the $BaCl_2$ treated WT condition, $p < 0.05$.

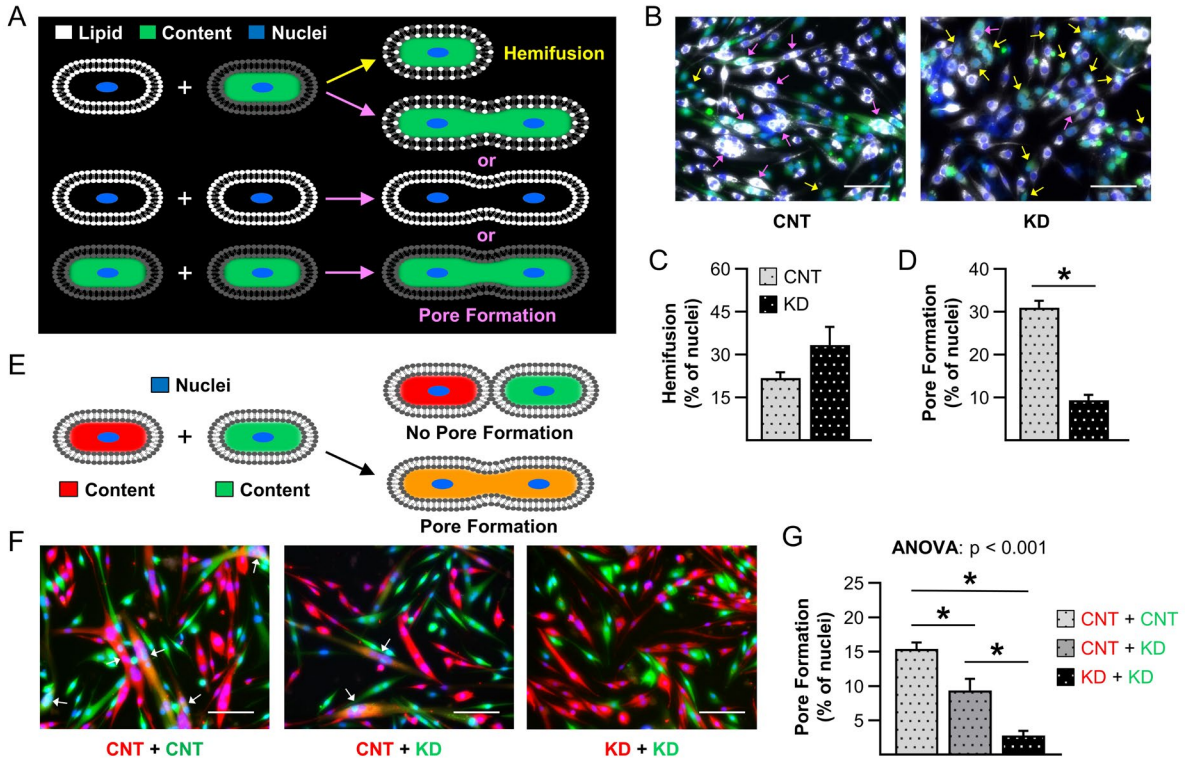

Fig. 9. The loss of TRIM28 inhibits the process of fusion pore formation but not hemifusion. Primary myoblasts were infected with a lentivirus expressing either scrambled shRNA (CNT) or shRNA targeting Trim28 (KD) and then differentiated for 24 hours. (**A-B**) CNT and KD myoblasts were detached and briefly labeled with either an intracellular content probe or a lipid membrane probe. The separately labeled cells were then mixed and differentiated for an additional 30 hours. Mononucleated cells that were positive for both probes were classified as having only undergone hemifusion (yellow arrows), whereas multinucleated were classified as having undergone fusion pore formation (pink arrows). (**C-D**) Quantification of the proportion of nuclei in cells that had undergone (C) only hemifusion, or (D) fusion pore formation. (**E-F**) CNT and KD myoblasts were detached, separated into two sub-groups, and labeled with a red- or green-fluorescent intracellular content probe. The separately labeled cells were mixed as indicated in F and differentiated for an additional 24 hours. Multinucleated cells that were positive for both probes (white arrows) were defined as having undergone fusion pore formation. (**G**) Quantification of the proportion of nuclei in cells that had undergone fusion pore formation during heterologous fusion. Values are group means + SEM, n = 4/group with each sample representing an independent line of isolated primary myoblasts. Data were analyzed with a Student's t-tests (B-C) or one-way ANOVA (G). * indicates a significant difference between the indicated groups, $p < 0.05$. Scale bars = 50 µm.

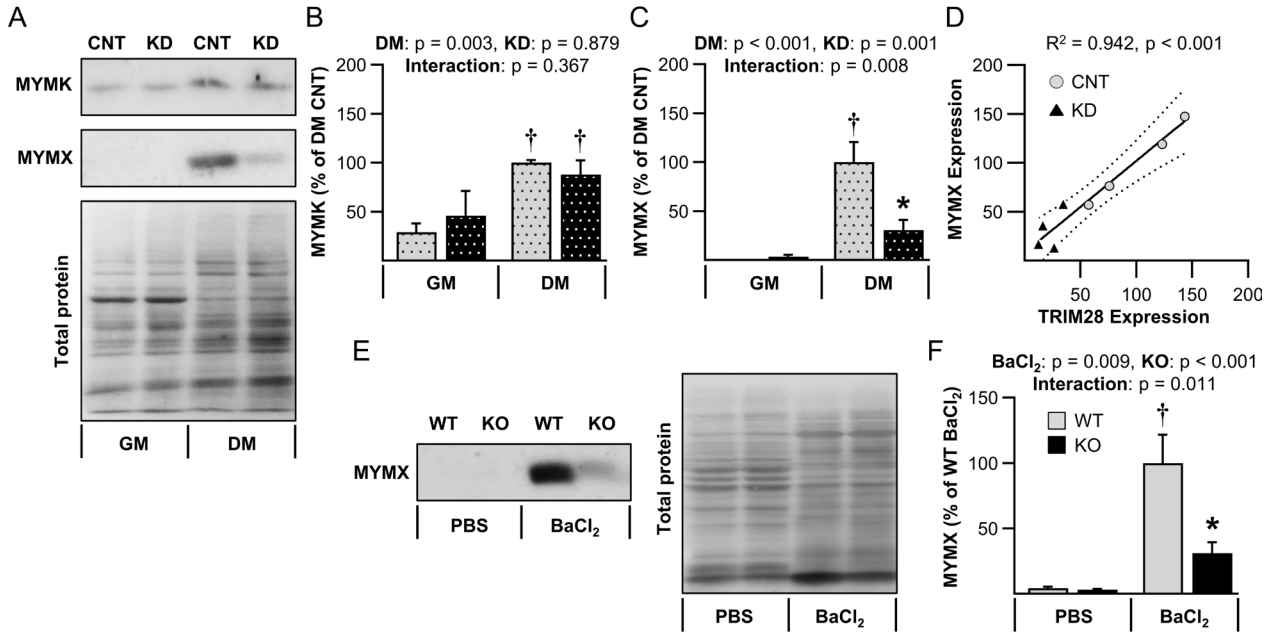

Fig. 10. The loss of TRIM28 inhibits the induction of MYMX expression during differentiation and injury-induced myogenesis. (**A-C**) As in Fig. 6, primary myoblasts were infected with lentivirus expressing scrambled shRNA (CNT) or shRNA targeting Trim28 mRNA (KD). The infected cells were cultured in growth media (GM) or differentiation media (DM) for 2 days and subjected to western blot analysis of myomaker (MYMK) and myomixer (MYMX). (**D**) Linear regression analysis of MYMX and TRIM28 expression from the infected cells that had been cultured in DM for 2 days (dashed lines represent the 95% confidence intervals). See Fig. 6 for the western blot analysis of TRIM28. (**E-F**) Tibialis anterior muscles from wild-type (WT) and tamoxifen-inducible satellite cell-specific TRIM28 knockout (KO) mice were collected at 3 days post-injury with $BaCl_2$ and subjected to western blot analysis of MYMX. Values are group means + SEM, n = 4-6/group with each sample representing an independent animal or line of isolated primary myoblasts. Data in B-D, and F were analyzed with two-way repeated-measures ANOVA. * indicates a significant effect of genotype within a given condition, † significant effect of DM or $BaCl_2$ within a given genotype, $p < 0.05$. Scale bars = 50 µm.

Supplementary Materials

Figs. S1-S10 and Table S1 can be found in the file entitled "supplementary materials".